

Shell-model calculations of nuclei around mass 130E. Teruya,^{1,*} N. Yoshinaga,^{1,†} K. Higashiyama,^{2,‡} and A. Odahara^{3,§}¹*Department of Physics, Saitama University, Saitama City 338-8570, Japan*²*Department of Physics, Chiba Institute of Technology, Narashino, Chiba 275-0023, Japan*³*Department of Physics, Osaka University, Osaka 560-0043, Japan*

(Received 26 May 2015; published 21 September 2015)

Shell-model calculations are performed for even-even, odd-mass, and doubly-odd nuclei of Sn, Sb, Te, I, Xe, Cs, and Ba isotopes around mass 130 using the single-particle space made up of valence nucleons occupying the $0g_{7/2}$, $1d_{5/2}$, $2s_{1/2}$, $0h_{11/2}$, and $1d_{3/2}$ orbitals. The calculated energies and electromagnetic transitions are compared with the experimental data. In addition, several typical isomers in this region are investigated.

DOI: [10.1103/PhysRevC.92.034320](https://doi.org/10.1103/PhysRevC.92.034320)

PACS number(s): 21.10.Ky, 21.60.Cs, 23.20.Lv, 27.60.+j

I. INTRODUCTION

The nuclear shell model (SM) remains vigorous as one of the most fundamental approaches for a microscopic description of nuclear structure. It has been very successful to understand structure of light and medium mass nuclei below mass 100. However, there are a couple of problems when the SM is applied to nuclei above mass 100. The main problem is the rapidly expanding dimension of the SM space as the number of valence nucleons increases. The SM dimension of typical nuclei around mass 130 amounts to more than 10^{11} , which overwhelmingly exceeds the number of configurations tractable with the present computing power. One needs to settle down this problem when the SM is applied to nuclei above mass 100. For example, the Monte Carlo shell model is one of the promising methods and attracts considerable attention, although it takes a lot of computational time [1,2]. In contrast, the conventional diagonalization approach using the Lanczos diagonalization method requires a truncation of the SM space [3,4].

For nuclei of mass number around 130, systematic experimental and theoretical investigations have been made in recent years. In this region, various characteristic phenomena due to the change of the nuclear structure have been known. One of the phenomena is the appearance of the doublet bands in doubly-odd nuclei, which are almost energetically degenerate $\Delta I = 1$ bands with the same parity [5–7]. In addition, large S -shaped bending of moments of inertia, called the backbending phenomenon, have been found in many nuclei [8]. This phenomenon is understood as crossing of the S band and the ground band. Moreover, isomers signaling changes in nuclear structure are present. For example, in even-even Sn isotopes, 10^+ isomers are present systematically [9]. Very recently new isomeric states have been found in ^{135}La [10] and ^{136}La [11], but the nature of these isomers still needs to be unveiled.

As for theoretical investigations, there exist several SM like approaches which systematically treat a large number of nuclei in this mass region [12–16]. In Refs. [12–14], the pair-truncated shell-model (PTSM) was applied for even-even, odd-mass, and doubly-odd nuclei. Energy levels and transition rates were calculated assuming all single-particle orbitals within the 50-82 shell. The interplay between the single-particle motion and the collective motion was investigated. Moreover, the staggering of electromagnetic transition rates for doublet bands was analyzed to find the existence of the chopsticks configurations [17–19], whose configurations have been also confirmed by a simplified model called the *quadrupole coupling model* [20].

Xe isotopes in the region around mass 130 were calculated using the SM in a truncated space assuming a few valence orbitals within the 50-82 shell [21]. Low-lying energy levels were well reproduced, but some high-spin states were only fairly reproduced due to a cutoff of single-particle orbitals.

In the present work SM calculations are carried out for even-even, odd-mass, and doubly-odd nuclei of Sn, Sb, Te, I, Xe, Cs, and Ba isotopes around mass 130. One major shell with all the five single-particle orbitals, $0g_{7/2}$, $1d_{5/2}$, $2s_{1/2}$, $0h_{11/2}$, and $1d_{3/2}$ are taken between the magic numbers 50 and 82. Here a phenomenological interaction is employed, which mainly consists of the pairing plus quadrupole-quadrupole interactions. First, the Hamiltonian in each neutron or proton space is diagonalized separately, and appropriate numbers of states from the lowest energy are employed for a model space truncation. Then the total Hamiltonian of neutrons and protons is diagonalized in the truncated space. After checking the convergence by increasing the number of states in each neutron or proton space, theoretical energy spectra and electromagnetic transition rates are compared with the experimental observations. Finally, structure of some intriguing nuclei and some isomeric states are investigated and structural changes in configuration space of the yrast states around the isomeric states are discussed. In order to analyze the structure of these isomeric states, the PTSM is employed.

This paper is organized as follows. Section II provides the general framework of the present SM study. The energy levels and the electromagnetic transitions in each nucleus are presented and compared with experiment in Sec. III. In this section, analyses of some isomeric states are also given. Finally

*teruya@nuclei.th.phy.saitama-u.ac.jp

†yoshinaga@phy.saitama-u.ac.jp

‡koji.higashiyama@it-chiba.ac.jp

§odahara@phys.sci.osaka-u.ac.jp

this work is summarized and conclusions are given in Sec. IV. Explicit formulas for two-body matrix elements are given in the Appendix.

II. THEORETICAL FRAMEWORK

A. Hamiltonian and single-particle energies

The nuclear structure of Sn, Sb, Te, I, Xe, Cs, and Ba isotopes is studied in terms of the SM. The model space used in the present calculation includes the $0g_{7/2}$, $1d_{5/2}$, $2s_{1/2}$, $0h_{11/2}$, and $1d_{3/2}$ orbitals in the major shell between the magic numbers 50 and 82. As an effective interaction, an extended pairing plus quadrupole-quadrupole interaction is employed. The effective shell-model Hamiltonian is given by

$$\hat{H} = \hat{H}_\nu + \hat{H}_\pi + \hat{H}_{\nu\pi}, \quad (1)$$

where \hat{H}_ν , \hat{H}_π , and $\hat{H}_{\nu\pi}$ represent neutron, proton, and neutron-proton interactions, respectively. The interactions among like nucleons are expressed as

$$\hat{H}_\tau = \hat{H}_{c\tau} + \hat{H}_{h\tau}. \quad (2)$$

The first term $\hat{H}_{c\tau}$ ($\tau = \nu$ or π) represents the conventional pairing plus quadrupole interaction, which consists of spherical single-particle energies, the monopole-pairing (*MP*) interaction, the quadrupole-pairing (*QP*) interaction, and the quadrupole-quadrupole (*QQ*) interaction,

$$\begin{aligned} \hat{H}_{c\tau} = & \sum_{jm} \varepsilon_{j\tau} c_{jm\tau}^\dagger c_{jm\tau} \\ & - G_{0\tau} \hat{P}_\tau^\dagger(0) \hat{P}_\tau(0) - G_{2\tau} \hat{P}_\tau^\dagger(2) \cdot \hat{P}_\tau(2) - \kappa_\tau : \hat{Q}_\tau \cdot \hat{Q}_\tau : , \end{aligned} \quad (3)$$

where $::$ represents the normal ordering. Here $c_{jm\tau}^\dagger$ and $c_{jm\tau}$ are the nucleon creation and annihilation operators, respectively, and (jm) stands for a shorthand notation of all the quantum numbers to uniquely specify a harmonic-oscillator basis state $|n\ell jm\rangle$. The monopole pair-creation operator $\hat{P}_\tau^\dagger(0)$, the quadrupole pair-creation operator $\hat{P}_{M\tau}^\dagger(2)$, and the quadrupole operator $\hat{Q}_{M\tau}$ are defined by

$$\hat{P}_\tau^\dagger(0) = \sum_j \frac{\sqrt{2j+1}}{2} A_{0\tau}^\dagger(jj), \quad (4)$$

$$\hat{P}_{M\tau}^\dagger(2) = \sum_{j_1 j_2} Q_{j_1 j_2} A_{M\tau}^\dagger(2)(j_1 j_2), \quad (5)$$

$$\hat{P}_{M\tau}^{(2)} = (-)^M \{ \hat{P}_{-M\tau}^\dagger(2) \}^\dagger, \quad (6)$$

$$\hat{Q}_{M\tau} = \sum_{j_1 j_2} Q_{j_1 j_2} [c_{j_1\tau}^\dagger \tilde{c}_{j_2\tau}^{(2)}]_M, \quad (7)$$

with

$$\tilde{c}_{jm\tau} = (-1)^{j-m} c_{j-m\tau}, \quad (8)$$

$$Q_{j_1 j_2} = -\frac{\langle j_1 || r^2 Y^{(2)} || j_2 \rangle}{\sqrt{5}}. \quad (9)$$

Here the creation operator of a pair of like-nucleons in the orbitals j_1 and j_2 with the total angular momentum J and its

projection M is constructed by

$$\begin{aligned} A_M^\dagger(J)(j_1 j_2) &= \sum_{m_1 m_2} (j_1 m_1 j_2 m_2 | JM) c_{j_1 m_1}^\dagger c_{j_2 m_2}^\dagger \\ &= [c_{j_1}^\dagger c_{j_2}^\dagger]_M^{(J)}, \end{aligned} \quad (10)$$

where $(j_1 m_1 j_2 m_2 | JM)$ stands for a Clebsch-Gordan coefficient. Here isospin notation τ has been skipped.

The second term $\hat{H}_{h\tau}$ in Eq. (2) represents newly introduced higher-order interactions, which consist of higher multipole-pairing (*HMP*) interactions,

$$\hat{H}_{h\tau} = - \sum_{L=4,6,8,10} G_{L\tau} \hat{P}_\tau^\dagger(L) \cdot \hat{P}_\tau^{(L)}. \quad (11)$$

Here the positive-parity multipole pair-creation operator, $\hat{P}_\tau^\dagger(L)$ ($L = 4, 6, 8, 10$), is defined as

$$\hat{P}_{M\tau}^\dagger(L) = \sum_{j_1 j_2} H_{j_1 j_2}^{(L)} A_{M\tau}^\dagger(L)(j_1 j_2), \quad (12)$$

with

$$H_{j_1 j_2}^{(L)} = -\frac{\langle j_1 || Y^{(L)} || j_2 \rangle}{\sqrt{2L+1}} \quad (13)$$

and

$$\hat{P}_{M\tau}^{(L)} = (-1)^M \{ \hat{P}_{-M\tau}^\dagger(L) \}^\dagger. \quad (14)$$

In other words each higher multipole-pairing operator is an extension of the quadrupole pair-creation operator without radial dependence.

The interaction between neutrons and protons $\hat{H}_{\nu\pi}$ is given as

$$\hat{H}_{\nu\pi} = -\kappa_{\nu\pi} \hat{Q}_\nu \cdot \hat{Q}_\pi, \quad (15)$$

where \hat{Q}_τ is the quadrupole operator defined by Eq. (7). Harmonic-oscillator states are used as the single-particle basis states with the oscillator parameter $b = \sqrt{\hbar/(M\omega)}$.

In the present work valence neutrons (protons) are treated as holes (particles) relative to the traditional cores of magic numbers 82 (50). The adopted single-particle energies for protons and single-hole energies for neutrons are listed in Table I. These single-particle energies are adopted from the experimental energy levels of ^{133}Sb (proton single-particle energies) and ^{131}Sn (neutron single-particle energies). As for the neutron $0h_{11/2}$ orbital and the proton $0g_{7/2}$ orbital, it is assumed that the energy of the single-particle orbital changes linearly with the numbers of valence neutron holes and proton

TABLE I. Adopted single-particle energies ε_τ ($\tau = \nu$ or π) for neutron holes and proton particles (in MeV). The energies for the neutron $0h_{11/2}$ and the proton $0g_{7/2}$ orbitals are changed linearly with numbers of valence neutron holes (N_ν) and proton particles (N_π). Definitions of $\varepsilon_\nu(h_{11/2})$ and $\varepsilon_\pi(g_{7/2})$ are given in the text.

j	$0g_{7/2}$	$1d_{5/2}$	$2s_{1/2}$	$0h_{11/2}$	$1d_{3/2}$
ε_ν	2.434	1.655	0.332	$\varepsilon_\nu(h_{11/2})$	0.000
ε_π	$\varepsilon_\pi(g_{7/2})$	0.962	3.000	2.791	2.440

TABLE II. Strengths of adopted two-body interactions between neutrons (ν - ν), protons (π - π), and neutrons and protons (ν - π). G_0 and G_2 indicate the strengths of the monopole (MP) and quadrupole-pairing (QP) interactions between like nucleons. G_L ($L = 4, 6, 8, 10$) denote the strengths for higher multipole-pairing (HMP) interactions between like nucleons. The κ_2 's indicate the strengths of the quadrupole-quadrupole (QQ) interactions between like and unlike nucleons. The strengths of MP and HMP interactions are given in units of MeV. The strengths of QP and QQ interactions are given in units of MeV/b^4 using the oscillator parameter b . Blanks mean that no strengths are employed.

	G_0	G_2	G_4	G_6	G_8	G_{10}	κ_2
ν - ν	0.170	0.018	-0.50	-2.00	-6.15	-14.0	0.010
π - π	0.165	0.007	0.20	0.10			0.055
ν - π							-0.100

particles. They are determined (in MeV) as follows:

$$\epsilon_\nu(h_{11/2}) = -0.46\bar{N}_\nu + 0.10N_\pi + 0.525, \quad (16)$$

$$\epsilon_\pi(g_{7/2}) = 0.06\bar{N}_\nu, \quad (17)$$

where \bar{N}_ν represents the number of valence neutron holes and N_π the number of valence proton particles. The number dependence of $\epsilon_\nu(h_{11/2})$ conforms with the experimentally suggested value when $N_\pi = 0$ and $\bar{N}_\nu = 1$ (^{131}Sn nucleus). This number dependence is introduced for a better reproduction of the low-lying negative-parity states of odd-mass nuclei after adjusting two-body interactions. Similarly, the number dependence of $\epsilon_\pi(g_{7/2})$ is given for a better description of energy spectra for even-even and odd-mass nuclei.

Two-body effective interactions are determined as follows: Since the energy spacings between the positive-parity states for odd-mass nuclei depend largely on the quadrupole-quadrupole interaction among like nucleons, these interaction strengths are adjusted to fit to the experimental excitation energies of the first excited states with positive parity in odd-mass nuclei. The strengths of other two-body interactions are determined so as to reproduce the energy levels of the yrast and other low-lying states of even-even nuclei. Effective interactions are basically determined by employing Sn isotopes ($\bar{N}_\nu \leq 5$), Te isotopes ($\bar{N}_\nu \leq 4$), I isotopes ($\bar{N}_\nu \leq 3$), and Xe isotopes ($\bar{N}_\nu \leq 2$). Cs and Ba isotopes are basically not used for fitting. In the present work no strengths for the proton $G_{8\pi}$ and $G_{10\pi}$ are assumed, since they only affect the high-lying states, for which experimental data are scarcely known.

The strengths of adopted two-body interactions are listed in Table II. Only one set of two-body interactions are applied to all the nuclei considered in this work.

B. Truncation scheme

In the medium and heavy nuclei whose mass are over 100, due to its huge dimension of the SM space, it is hard to perform a complete diagonalization of the Hamiltonian for the SM calculations. Thus some kinds of compromise is necessary by somehow decreasing the dimension of the SM space.

To this end, the SM calculations are performed according to the following prescription. This truncation method is inherent to the present approach by utilizing the fact that only a quadrupole-quadrupole interaction (QQ interaction) is assumed between neutrons and protons and also that the QQ interaction is weak in this region. Before diagonalizing the total Hamiltonian in Eq. (1), the following steps are taken. First, the neutron interaction \hat{H}_ν in the neutron space is diagonalized and all the eigenenergies and eigenwavefunctions are obtained in the neutron system,

$$\hat{H}_\nu|i, I_i M_i\rangle_\nu = E_\nu(i, I_i)|i, I_i M_i\rangle_\nu, \quad (18)$$

where i takes $i = 1, \dots, L_\nu$ and I_i is spin of the i th state and L_ν is the maximum number of possible states. M_i represents the angular momentum projection and $M_i = 0$ is taken for even-particle systems and $M_i = 1/2$ for odd-particle systems. The eigenenergies are ordered in increasing order as $E_\nu(1, I_1) \leq E_\nu(2, I_2) \leq \dots$. Next, the proton interaction \hat{H}_π is diagonalized and all the eigenenergies and eigenwavefunctions are obtained in the proton system,

$$\hat{H}_\pi|j, I_j M_j\rangle_\pi = E_\pi(j, I_j)|j, I_j M_j\rangle_\pi, \quad (19)$$

where j takes $j = 1, \dots, L_\pi$ and eigenenergies are ordered in increasing order $E_\pi(1, I_1) \leq E_\pi(2, I_2) \leq \dots$. Then, by angular momentum coupling a neutron state and a proton state, a neutron-proton basis state is obtained:

$$\begin{aligned} |IM, \alpha\rangle &= [|i, I_i\rangle_\nu \times |j, I_j\rangle_\pi]_M^{(I)} \\ &= \sum_{M_i M_j} (I_i M_i I_j M_j | IM) |i, I_i M_i\rangle_\nu |j, I_j M_j\rangle_\pi. \end{aligned} \quad (20)$$

Finally, the total Hamiltonian is diagonalized as follows;

$$\hat{H}|\Phi(I_k; k)\rangle = E(I_k, k)|\Phi(I_k; k)\rangle. \quad (21)$$

Here k represents the k th state with total spin I_k in the total neutron-proton space and the eigenstate $|\Phi(I_\ell; \ell)\rangle$ is expressed as $|\Phi(I_\ell; \ell)\rangle = \sum_\alpha v_{\ell\alpha}^{(I)} |I, \alpha\rangle$ using the basis states in the Hamiltonian in Eq. (20). The coefficients $v_{\ell\alpha}^{(I)}$ are obtained by diagonalizing Eq. (1).

In the following calculation we cut off the number of levels to calculate eigenenergies and eigenwave functions in a neutron-proton system and take a common number of levels (L_c) from the lowest state in each neutron or proton space, separately,

$$i, j = 1, \dots, L_c. \quad (22)$$

The validity of this truncation of the model space is checked in Sec. III A.

C. Electromagnetic transitions

The electromagnetic transition rates are given as follows. The $E2$ transition rate is calculated as

$$B(E2; I_i \rightarrow I_f) = \frac{1}{2I_i + 1} |\langle \Phi(I_f; f) | \hat{T}(E2) | \Phi(I_i; i) \rangle|^2, \quad (23)$$

where $|\Phi(I_i; i)\rangle$ represents the wave function in Eq. (21). Here the $E2$ transition operator is defined as

$$\hat{T}(E2) = e_\nu \hat{Q}_\nu + e_\pi \hat{Q}_\pi, \quad (24)$$

where e_τ ($\tau = \nu$ or π) represents the effective charge of the nucleon, and the operator \hat{Q}_τ is the quadrupole operator defined by Eq. (7) with the oscillator parameter $b = 1.005A^{1/6}$ fm with A being mass number. Effective charges are chosen as $e_\nu = -0.60e - 0.10\bar{N}_\nu e$ for neutrons and as $e_\pi = +1.80e - 0.05N_\pi e$ for protons. These values were adjusted to reproduce experimental $B(E2)$ values in single-closed nuclei. Note that the neutron effective charge is chosen to be negative, as valence neutrons are treated as holes.

The $M1$ transition rate is calculated as

$$B(M1, I_i \rightarrow I_f) = \frac{1}{2I_i + 1} |\langle \Phi(I_f; f) | \hat{T}(M1) | \Phi(I_i; i) \rangle|^2. \quad (25)$$

Here the $M1$ transition operator is defined as

$$\hat{T}(M1) = \mu_N \sqrt{\frac{3}{4\pi}} \sum_\tau [g_{\ell\tau} \hat{j}_\tau + (g_{s\tau} - g_{\ell\tau}) \hat{s}_\tau], \quad (26)$$

where μ_N is the nuclear magneton. The $g_{\ell\nu}$ and $g_{\ell\pi}$ ($g_{s\nu}$ and $g_{s\pi}$) represent the gyromagnetic ratios for orbital angular momenta (spins) for neutrons and protons, respectively. The operators \hat{j}_τ and \hat{s}_τ stand for the angular momentum and spin operators, respectively. The adopted gyromagnetic ratios for orbital angular momenta are $g_{\ell\nu} = 0.00$, $g_{\ell\pi} = 1.00$, and those for spin are $g_{s\nu} = -2.68$ and $g_{s\pi} = 3.91$, which are free-nucleon g factors attenuated by a factor of 0.7.

D. Electromagnetic moments

The magnetic dipole moment is calculated as

$$\mu(I_i) = \langle \Phi(I_i, M = I_i; i) | \hat{\mu}_0 | \Phi(I_i, M = I_i; i) \rangle. \quad (27)$$

The $\hat{\mu}_0$ represents the third component of the magnetic dipole operator, which is written as

$$\hat{\mu}_M = \mu_N \sum_\tau [g_{\ell\tau} \hat{j}_{M\tau} + (g_{s\tau} - g_{\ell\tau}) \hat{s}_{M\tau}], \quad (28)$$

where the operators \hat{j}_τ and \hat{s}_τ and the gyromagnetic ratios are taken to be the same as used in the $M1$ transition rates.

The electric quadrupole moment is calculated as

$$Q(I_i) = \langle \Phi(I_i, M = I_i; i) | \hat{Q}_0 | \Phi(I_i, M = I_i; i) \rangle. \quad (29)$$

Here the electric quadrupole operator is given by

$$\hat{Q}_M = \sqrt{\frac{16\pi}{5}} (e_\nu \hat{Q}_{M\nu} + e_\pi \hat{Q}_{M\pi}). \quad (30)$$

The quadrupole operator \hat{Q}_τ , the effective charge e_τ , and the oscillator parameter b are taken to be the same as used for the $E2$ transition rates.

E. Occupation numbers in orbital j

The occupation number in the single-particle orbital j for the state $|\Phi(I_i; i)\rangle$ is evaluated as

$$v^2(j) = \langle \Phi(I_i; i) | \hat{n}_j | \Phi(I_i; i) \rangle, \quad (31)$$

where the particle number operator \hat{n}_j in the j orbital is defined as

$$\hat{n}_j = \sum_m c_{jm}^\dagger c_{jm} = -\sqrt{2j+1} [c_j^\dagger \tilde{c}_j]^{(0)}. \quad (32)$$

III. NUMERICAL RESULTS

Using the interaction strengths determined above, the energy spectra and transition rates for Sn, Sb, Te, I, Xe, Cs, and Ba isotopes are calculated. First, we check the validity of truncation of the model space mentioned in Sec. III A. Then we compare the energy spectrum and electromagnetic transition rates in experiment and theory for each nucleus in Sec. III B. Finally, we discuss some intriguing nuclei which are essential to determine two-body effective interactions and also analyze some isomers in Sec. III C. Here wave functions of isomeric states are analyzed using the PTSM and structural changes around isomeric states are examined.

For even-even nuclei, the yrast states and the yrare states with positive parity are presented in the present study. For other nuclei, only the yrast states are presented. Energy levels up to 5, 3, and 1 MeV are calculated for even-even, odd-mass, and doubly-odd nuclei, respectively. For experimental data, only those states whose energy, spin, and parity are assigned in experiment are shown in the figure. Ambiguous states are shown with parentheses.

A. Checking the cutoff

In the present work the SM space is cut off. Here the validity of its truncation of the model space is checked. Figure 1(a) shows the comparison of the calculated energy spectra between the $L_c = 500$ truncation and the $L_c = 1000$ truncation for ^{135}Ba . This nucleus of three valence neutron holes and six valence protons has $L_\nu = 245$ for neutron positive-parity states, $L_\nu = 203$ for neutron negative-parity states, $L_\pi = 31124$ for proton positive-parity states, and $L_\pi = 30636$ for proton negative-parity states. These are dimensions of states with angular momentum projection $M = 0$ (for even-particle systems) and $M = 1/2$ (for odd-particle systems), respectively, in each neutron or proton space.

Figure 1(b) shows the same as in Fig. 1(a), but for ^{136}Ba . ^{136}Ba has $L_\nu = 36$ neutron positive-parity states, $L_\nu = 20$ neutron negative-parity states. The number of states for the proton system is the same as in ^{135}Ba .

Figure 1(c) shows the same spectra as in Fig. 1(a), but for ^{132}Ba . This nucleus has six valence neutron holes and six valence proton particles. The nucleus has the largest SM dimension among nuclei treated in this paper. It is seen that $L_c = 500$ truncation is enough for these nuclei to have energy convergence. In general, excited energies in the $L_c = 1000$ truncation are a bit lower than those in the $L_c = 500$ truncation. This is because higher energy states need a higher number of neutron-proton basis states than the low-lying states.

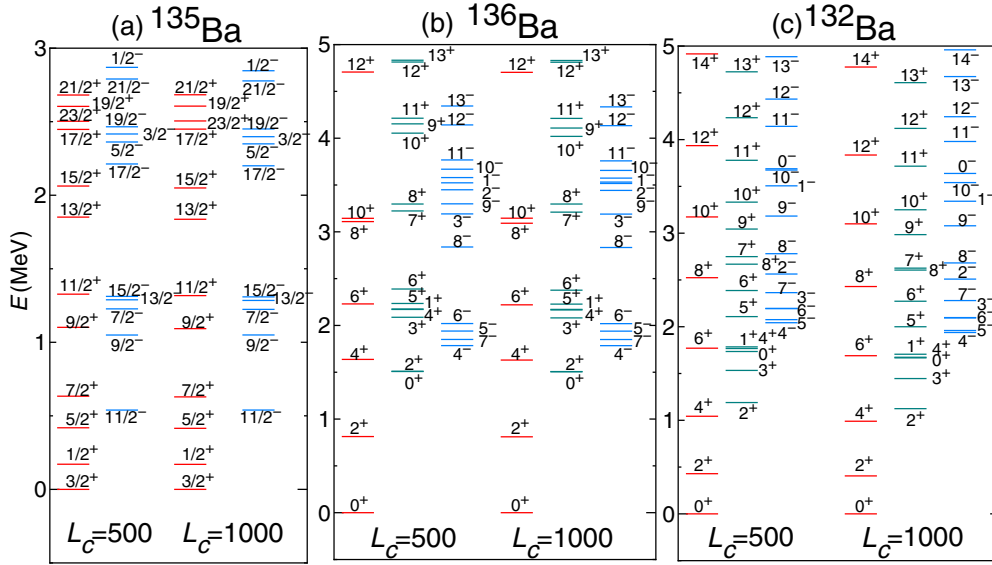


FIG. 1. (Color online) Comparison between the spectra in which the number of levels (L_c) for diagonalization is limited to 500 ($L_c = 500$) and 1000 ($L_c = 1000$) for (a) ^{135}Ba , (b) ^{136}Ba , and (c) ^{132}Ba .

In the following all the calculations are performed with the truncation of $L_c = 500$.

B. Comparison between experiment and theory

1. Sn isotopes

Here $^{126-130}_{50}\text{Sn}$ isotopes are discussed. Figure 2 shows the theoretical spectra for Sn isotopes (single-closed nuclei) in comparison with the experimental spectra [22–29].

^{130}Sn is a semimagic nucleus with two valence neutron holes. This nucleus becomes a benchmark to test the neutron two-body interactions. The present calculation reproduces the feature of a spherical nucleus that the spacing between two neighboring yrast states becomes smaller and smaller as spin goes up from 0 to 10. Energies of the 4_1^+ and 6_1^+ states are not well reproduced. However, they would be adjusted to the experimental energies by changing $G_{4\nu}$ and $G_{6\nu}$ strengths. The detailed analysis is performed in Sec. III C for this nucleus.

In ^{128}Sn , the 6_1^+ state is not observed at present. The theoretical 6_1^+ state is predicted at 2.03 MeV. The spin-parity of the state at 2.26 MeV is experimentally assigned as either $(1)^-$ or $(2)^+$. The spin-parity of this state is presumed to be 2^+ since the 2_3^+ state and the 1_1^- state are predicted at 2.24 and 3.08 MeV, respectively, in this calculation.

In ^{126}Sn the experimental second 4^+ state at 3.42 is 1.33 MeV higher than the predicted 4_2^+ state. Therefore the experimental second 4^+ state might not correspond to the theoretical 4_2^+ state. Theoretically, several 4^+ states (not shown in the figure) are predicted at around 3.4 MeV.

In ^{127}Sn and ^{129}Sn , not only the low-lying states but also high-spin states are well reproduced. The spin-parity of the state at 1.53 MeV in ^{129}Sn is experimentally assigned as either $(7/2^-)$ or $(9/2^+)$. Theoretically, the $9/2_1^+$, $7/2_1^-$, and $7/2_2^-$ states are predicted at 1.53, 1.05, and 2.20 MeV, respectively. Thus the spin-parity of this state would be $9/2^+$.

In Table III the theoretical $B(E2)$ values of Sn isotopes among the low-lying states are compared with the experimental data [22–25,29–33]. The experimental values are well reproduced in general, although measured data are not as numerous. The 10_1^+ states of even-even Sn isotopes in this mass region are known to be isomers whose half-lives are few microseconds. The $B(E2; 10_1^+ \rightarrow 8_1^+)$ values are several times smaller than other transition rates among yrast states in the calculation. The detailed analyses of these states are performed in Sec. III C.

Table IV shows the theoretical magnetic dipole moments μ and electric quadrupole moments Q of Sn isotopes in comparison with the experimental data [22–25,29–35]. Experimental values are well reproduced in general, especially magnetic dipole moments. However, there are some discrepancies for quadrupole moments between theory and experiment. The theoretical quadrupole moment of the $11/2_1^-$ state in ^{127}Sn is 4.0 times smaller than the experimental one. The theoretical quadrupole moment of the 7_1^- state in ^{130}Sn agrees with the experimental value within the experimental error, but the sign, in theory, is opposite to that in experiment. In contrast, the magnetic moments of these two states agree with the experimental values.

It is a general feature that the calculated quadrupole moment of a state does not agree so well with the experimental data, but the calculated magnetic moment of the same state agrees with the experimental one well. This feature is commonly seen for other nuclear states discussed later.

2. Sb isotopes

Here $^{127-132}_{51}\text{Sb}$ isotopes are discussed. Figure 3 shows the theoretical spectra of Sb isotopes compared to the experimental data [22–25,29,39–42].

^{131}Sb has two valence neutron holes and one valence proton particle. Negative-parity states are predicted to be densely

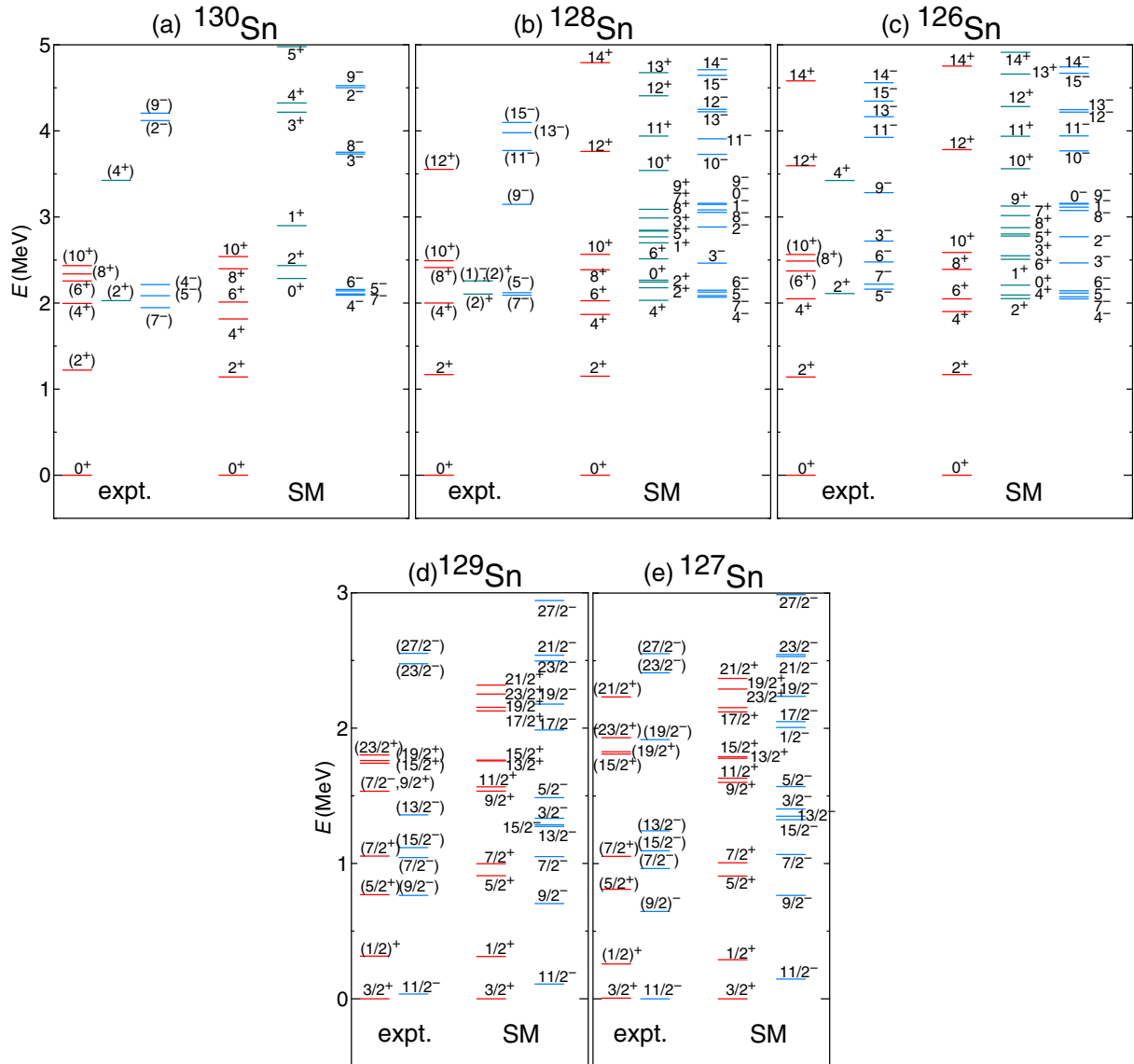


FIG. 2. (Color online) Comparison between the experimental spectra (expt.) and the shell-model results (SM) for Sn isotopes. The experimental data are taken from Refs. [22–29,36].

located at around 2.0 MeV in theory. The $23/2_1^+$ state is an isomer with a half-life of $1.1(2) \mu\text{s}$ [39]. This isomer is analyzed later in Sec. III C.

In ^{129}Sn , the $19/2_1^-$ state at 1.85 MeV is an isomer with a half-life of $17.7(1) \text{ min}$ [24]. Considering its long half-life, this state should be a spin-gap isomer [43]. Therefore states which can be easily connected by $E2$ or $M1$ transitions, like $15/2^-$ and $17/2^-$ states, should be located above the $19/2_1^-$ state even if the former states exist. However, calculated $15/2_1^-$ and $17/2_1^-$ states are located just below the $19/2_1^-$ state. To push up these $15/2_1^-$ and $17/2_1^-$ states above the $19/2_1^-$ state, neutron-proton two-body interactions beside the QQ interaction would be necessarily. The spin-parity of the state at 1.25 MeV is experimentally assigned as either $(3/2^+)$, $(5/2)$, or $(7/2^-)$. This state is inferred as the $5/2_2^+$ state since theoretical $5/2_2^+$, $7/2_1^+$, and $3/2_2^+$ states are predicted at 1.29, 1.89, and 1.82 MeV, respectively.

In ^{127}Sb , the experimentally assigned $(9/2^-)$ state at 2.85 MeV might not be the first $9/2^-$ state. Theoretically, the $9/2_1^-$ state is predicted at 1.93 MeV. Moreover, besides those shown in Fig. 3, many candidates for the $(9/2^-)$ state at 2.85 MeV are experimentally found above 1.9 MeV although spin and parity are not definitely assigned for most of them [29].

^{132}Sb is a one-neutron hole and one-proton particle system. This nucleus is a benchmark to check two-body neutron-proton interactions. Experimental energy of the 8_1^- state is found to be $0.0 + x \text{ keV}$, where x is estimated as $x = 150 \sim 250 \text{ keV}$ [25]. Thus this state is shown in the Fig. 3 assuming $x = 200$. The detailed analysis is performed in Sec. III C for this nucleus.

In ^{130}Sb , the spin-parity of the experimental ground state is 8^- . However, the spin-parity of the theoretical ground state is 4^+ and the 8_1^- state is calculated at 0.279 MeV. Theoretical negative-parity states are about 0.2 MeV higher than those states in experiment as a whole. These states could be lowered

TABLE III. Comparison between the experimental $B(E2)$ values (expt.) and the theoretical results (SM) for Sn isotopes (in W.u.). The experimental data are taken from Refs. [22–25,27,29–33,36,37].

^{126}Sn	Expt.	SM
$2_1^+ \rightarrow 0_1^+$	6.77(43)	7.40
$4_1^+ \rightarrow 2_1^+$		0.0615
$6_1^+ \rightarrow 4_1^+$		0.0688
$8_1^+ \rightarrow 6_1^+$		0.0419
$10_1^+ \rightarrow 8_1^+$		0.0151
^{127}Sn	Expt.	SM
$3/2_1^+ \rightarrow 1/2_1^+$		1.56
$5/2_1^+ \rightarrow 1/2_1^+$		0.102
$5/2_1^+ \rightarrow 3/2_1^+$		4.68
$19/2_1^+ \rightarrow 15/2_1^+$	1.00(10)	1.05
$23/2_1^+ \rightarrow 19/2_1^+$	0.417(5)	0.307
$9/2_1^- \rightarrow 11/2_1^-$		7.22
$7/2_1^- \rightarrow 9/2_1^-$		0.0340
$7/2_1^- \rightarrow 11/2_1^-$		4.98
^{128}Sn	Expt.	SM
$2_1^+ \rightarrow 0_1^+$	4.18(26)	4.09
$4_1^+ \rightarrow 2_1^+$		0.504
$6_1^+ \rightarrow 4_1^+$		0.642
$8_1^+ \rightarrow 6_1^+$		0.565
$10_1^+ \rightarrow 8_1^+$	0.341(17)	0.177
^{129}Sn	Expt.	SM
$3/2_1^+ \rightarrow 1/2_1^+$		1.11
$5/2_1^+ \rightarrow 1/2_1^+$		0.0328
$5/2_1^+ \rightarrow 3/2_1^+$		1.88
$19/2_1^+ \rightarrow 15/2_1^+$	1.4(6)	1.39
$23/2_1^+ \rightarrow 19/2_1^+$	1.39(10)	0.633
$9/2_1^- \rightarrow 11/2_1^-$		3.02
$7/2_1^- \rightarrow 9/2_1^-$		0.169
$7/2_1^- \rightarrow 11/2_1^-$		1.97
^{130}Sn	Expt.	SM
$2_1^+ \rightarrow 0_1^+$		1.52
$4_1^+ \rightarrow 2_1^+$		1.45
$6_1^+ \rightarrow 4_1^+$		1.43
$8_1^+ \rightarrow 6_1^+$		0.871
$10_1^+ \rightarrow 8_1^+$	0.38(4)	0.330
$5_1^- \rightarrow 7_1^-$	1.4(2)	0.695

by changing the single-particle energy of the neutron $h_{11/2}$ orbital and/or the $G_{6\nu}$ interaction. In the present scheme higher multipole interactions are necessary in addition to the quadrupole-quadrupole interactions between neutrons and protons to get the 8_1^- state as the ground state, which will be discussed in Sec. III C for ^{132}Sb .

In ^{130}Sb , positive-parity states are found at 0.005, 0.068, and 0.075 MeV in experiment, although spins of these states are not assigned. The 2_1^+ , 3_1^+ , 4_1^+ , and 5_1^+ states are calculated to be below 0.3 MeV. These theoretical states would correspond to the above experimental states. In the present calculation it is found that the 2_1^+ , 3_1^+ , 4_1^+ , and 5_1^+ states consist of the $(\nu d_{3/2}^{-1} h_{11/2}^{-2} \pi g_{7/2})$ configuration through the analysis of the occupation numbers.

It is presumed that the experimental $(2)^+$ state at 0.749 MeV is the second or third 2^+ state, since this experimental state is

TABLE IV. Comparison of the magnetic dipole moments μ (in μ_N) and the electric quadrupole moments Q (in eb) obtained by the shell model (SM) to the experimental data (expt.) for Sn isotopes. The experimental data are taken from Refs. [22–25,29–36,38].

^{126}Sn	μ		Q	
	Expt.	SM	Expt.	SM
2_1^+	-0.26(6)	-0.420		+0.0305
4_1^+		-0.957		-0.0388
6_1^+		-1.45		-0.0143
^{127}Sn	Expt.	SM	Expt.	SM
$3/2_1^+$	+0.757(4)	+0.801	+0.30(13)	+0.107
$5/2_1^+$		+0.110		-0.0765
$19/2_1^+$	-1.6(2)	-1.15		+0.239
$7/2_1^-$		-0.896		+0.0749
$9/2_1^-$		-1.10		+0.134
$11/2_1^-$	-1.329(7)	-1.34	+0.32(14)	+0.0797
^{128}Sn	Expt.	SM	Expt.	SM
2_1^+	(-)0.46(6)	-0.430		-0.0586
4_1^+		-0.966		-0.0764
6_1^+		-1.45		-0.0341
10_1^+	-2.0(4)	-2.43		+0.205
^{129}Sn	Expt.	SM	Expt.	SM
$3/2_1^+$	+0.754(6)	+0.803	+0.05(11)	+0.0943
$5/2_1^+$		+0.116		-0.0835
$7/2_1^-$		-0.899		+0.0773
$9/2_1^-$		-1.11		+0.313
$11/2_1^-$	-1.297(5)	-1.34	-0.18(17)	+0.150
^{130}Sn	Expt.	SM	Expt.	SM
2_1^+		-0.435		-0.102
4_1^+		-0.969		-0.114
6_1^+		-1.45		-0.0266
7_1^-	-0.381(3)	-0.513	-0.39(12)	+0.298

close to the calculated 2_2^+ (0.707 MeV) or 2_3^+ (0.781 MeV) states in energy. The 2_1^+ state and the 2_2^+ state were also predicted at about 0.3 MeV and at about 0.7 MeV, respectively, in Ref. [44].

In ^{128}Sb , the positive-parity band starting at the 5^+ state ($0.0 + x$ keV) is observed, where x is estimated as $x = 20$ keV [23]. The energy levels are shown in the figure using this value. The spin-parity of the experimental ground state is 8^- . However, the spin-parity of the theoretical one is 4^+ . The calculated 8_1^- state is located at 0.271 MeV. As discussed in ^{130}Sb , the modification of the single-particle energy of the neutron $h_{11/2}$ orbital and/or the $G_{6\nu}$ interaction would be necessary.

As for the doubly-odd Sb isotopes, a modification of the two-body interactions and/or single-particle energies in each nucleus is necessary for a better fitting with the experimental data.

Table V shows the theoretical $B(E2)$ values of Sb isotopes among the low-lying states in comparison with the experimental data [24,25,29,39–41,45]. Only a few experimental $B(E2)$ values are known. The largest discrepancy between the experimental data and the theoretical ones is seen in the $B(E2; 3_1^+ \rightarrow 4_1^+)$ value for ^{132}Sb . The theoretical value is 2.6 times larger than the experimental one [0.9(3) W.u.]. The

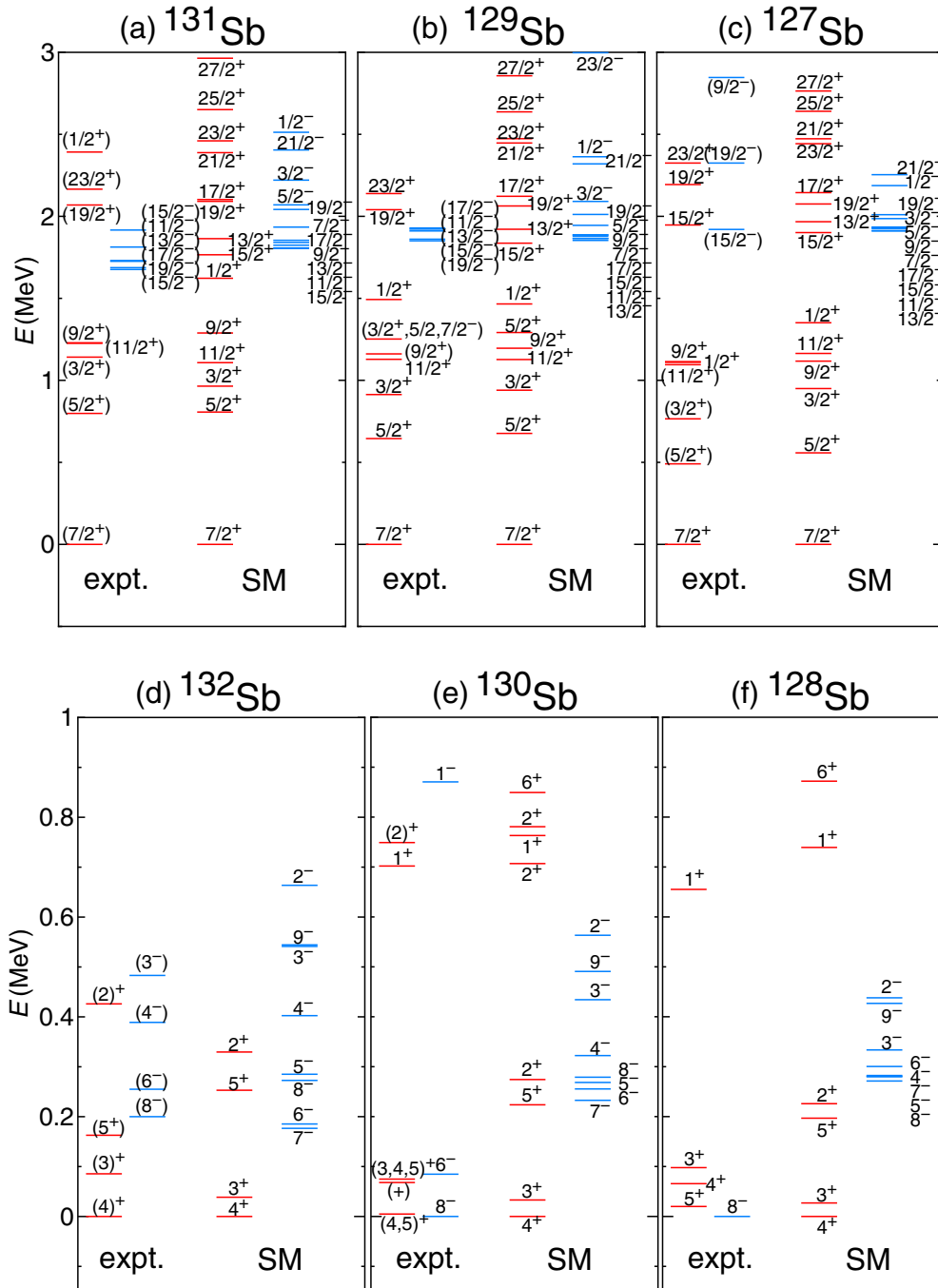


FIG. 3. (Color online) Comparison between the experimental spectra (expt.) and the SM results (SM) for Sb isotopes. The experimental data are taken from Refs. [22–25,29,39–42,47].

same transition rate was calculated using a SM in Ref. [46], whose value is 1.05 W.u. They used the proton effective charge $e_\pi = 1.55e$ and the neutron effective charge $e_\nu = 0$. Adopting the same effective charges in the present scheme, a similar result is obtained: $B(E2; 3_1^+ \rightarrow 4_1^+) = 1.12$ W.u.

In general, the present calculation predicts large $B(E2; 3/2_1^+ \rightarrow 7/2_1^+)$ values in odd-mass nuclei, which are not measured in experiment. For example, the $B(E2; 3/2_1^+ \rightarrow 7/2_1^+)$ value in ^{127}Sb is 17.1 W.u. It is inferred that the $7/2_1^+$ state mainly consists of the $|0^+\rangle_\nu \otimes |g_{7/2}\rangle_\pi$ configuration,

while the $3/2_1^+$ state mainly consists of the $|2^+\rangle_\nu \otimes |g_{7/2}\rangle_\pi$ configuration. Thus the $E2$ transition rates are expected to be large. Future experimental measurement is desired.

Table VI shows the theoretical magnetic dipole moments μ and electric quadrupole moments Q of Sb isotopes in comparison with the experimental data [22–24,29,34,35,38,39]. For these nuclei, only magnetic dipole moments are measured. Theoretical results are in good agreement with the experimental data. Differences between the experimental data and theoretical predictions are less than twice in magnitude.

TABLE V. Comparison between the experimental $B(E2)$ values (expt.) and the theoretical results (SM) for Sb isotopes (in W.u.). The experimental data are taken from Refs. [24,25,29,39–41,45].

^{127}Sb	Expt.	SM
$3/2_1^+ \rightarrow 5/2_1^+$		2.76
$3/2_1^+ \rightarrow 7/2_1^+$		17.1
$5/2_1^+ \rightarrow 7/2_1^+$		1.93
^{128}Sb	Expt.	SM
$3_1^+ \rightarrow 4_1^+$		5.57
$5_1^+ \rightarrow 4_1^+$		6.36
$5_1^+ \rightarrow 3_1^+$		0.00224
^{129}Sb	Expt.	SM
$3/2_1^+ \rightarrow 5/2_1^+$		1.91
$3/2_1^+ \rightarrow 7/2_1^+$		11.0
$5/2_1^+ \rightarrow 7/2_1^+$		1.45
$23/2_1^+ \rightarrow 19/2_1^+$	0.52(5)	0.969
^{130}Sb	Expt.	SM
$3_1^+ \rightarrow 4_1^+$		3.83
$2_1^+ \rightarrow 3_1^+$		1.53
$1_1^+ \rightarrow 2_1^+$		1.56
$13_1^+ \rightarrow 11_1^+$	1.81(20)	1.17
$6_1^- \rightarrow 8_1^-$	0.92(10)	1.24
^{131}Sb	Expt.	SM
$3/2_1^+ \rightarrow 5/2_1^+$		1.10
$3/2_1^+ \rightarrow 7/2_1^+$		4.92
$5/2_1^+ \rightarrow 7/2_1^+$		0.975
$23/2_1^+ \rightarrow 19/2_1^+$	0.54(11)	0.370
$19/2_1^- \rightarrow 15/2_1^-$	0.99(18)	0.840
^{132}Sb	Expt.	SM
$3_1^+ \rightarrow 4_1^+$	0.9(3)	2.37
$2_1^+ \rightarrow 3_1^+$	<8.1	0.752
$1_1^+ \rightarrow 2_1^+$	>0.0018	0.0748
$6_1^- \rightarrow 8_1^-$		0.429
$4_1^- \rightarrow 6_1^-$		1.34

3. Te isotopes

Here $^{128-134}_{52}\text{Te}$ isotopes are discussed. Figure 4 shows the theoretical spectra in Te isotopes compared to the experimental data [23–25,29,39,40,48–53].

^{134}Te is a single-closed nucleus with two valence protons. It is a suitable nucleus to check two-body interactions between protons. A detailed analysis is performed in Sec. III C for this nucleus.

In ^{132}Te , ^{130}Te , and ^{128}Te , small energy spacings between 10_1^+ and 8_1^+ states are well reproduced. Because of these small energy spacings, even if $B(E2; 10_1^+ \rightarrow 8_1^+)$ values are not so small, the 10_1^+ states in these nuclei become isomers with half-lives of 3.70(9) μs , 1.90(8) μs , and 0.37(3) μs , respectively [23,25,40].

In ^{132}Te , the experimental second 4^+ state at 2.76 MeV is much higher than the calculated one (1.93 MeV). There is a possibility that the 4^+ state at 2.76 MeV is not the second 4^+ state. Many energy levels are observed below 2.8 MeV in experiment although spins and parities of these states are not completely assigned. In fact, there are other calculated 4^+ states at 2.39 and 2.72 MeV (not shown in the figure).

TABLE VI. Comparison of the magnetic dipole moments μ (in μ_N) and the electric quadrupole moments Q (in eb) obtained by the shell model (SM) to the experimental data (expt.) for Sb isotopes. The experimental data are taken from Refs. [22–24,29,34,35,38,39].

^{127}Sb	μ		Q	
	Expt.	SM	Expt.	SM
$3/2_1^+$		+1.65		-0.277
$5/2_1^+$		+3.67		-0.494
$7/2_1^+$	2.697(6)	+2.25		-0.590
^{128}Sb	Expt.	SM	Expt.	SM
2_1^+		+1.48		-0.283
3_1^+		+2.25		-0.434
4_1^+		+2.35		-0.475
8_1^-	1.3(2)	+0.680		-0.237
^{129}Sb	Expt.	SM	Expt.	SM
$3/2_1^+$		+1.81		-0.232
$5/2_1^+$		+3.68		-0.415
$7/2_1^+$	2.79(2)	+2.27		-0.495
^{130}Sb	Expt.	SM	Expt.	SM
2_1^+		+1.53		-0.226
3_1^+		+2.29		-0.373
4_1^+		+2.39		-0.402
6_1^-		-0.0168		+0.196
7_1^-		+0.354		+0.0354
8_1^-		+0.686		-0.0943
^{131}Sb	Expt.	SM	Expt.	SM
$3/2_1^+$		+1.96		-0.186
$5/2_1^+$		+3.74		-0.337
$7/2_1^+$	2.89(1)	+2.31		-0.403
^{132}Sb	Expt.	SM	Expt.	SM
2_1^+		+1.61		-0.186
3_1^+		+2.37		-0.309
4_1^+		+2.45		-0.328
4_1^-		-0.991		+0.254
6_1^-		-0.0259		+0.210
8_1^-		+0.715		-0.00788

One of them might correspond to the experimental 4^+ state at 2.76 MeV.

In ^{133}Te , ^{131}Te , and ^{129}Te , many states are predicted above 1.5 MeV besides those shown in the figure. In ^{131}Te and ^{129}Te , theoretical negative-parity levels are over 0.1 MeV higher than the experimental ones as a whole. They could be adjusted by changing the single-particle energy of the neutron $h_{11/2}$ orbital. For example, in the case of ^{129}Te , the adopted single-particle energy of the neutron $h_{11/2}$ orbital is $\epsilon_v(h_{11/2}) = -1.575$ MeV in the present calculation, but adoption of $\epsilon_v(h_{11/2}) = -2.10$ MeV would be the best choice for this nucleus alone.

In ^{129}Te , the first $9/2^+$ is experimentally observed at 1.73 MeV; however, it is inferred that this state is not the first $9/2^+$ state since the $9/2_1^+$ state is predicted at 1.34 MeV in the present calculation. In fact, in experiment there exist several candidates below 1.73 MeV, which are seemingly $9/2^+$ states [29]. Using the interacting boson-fermion model, the

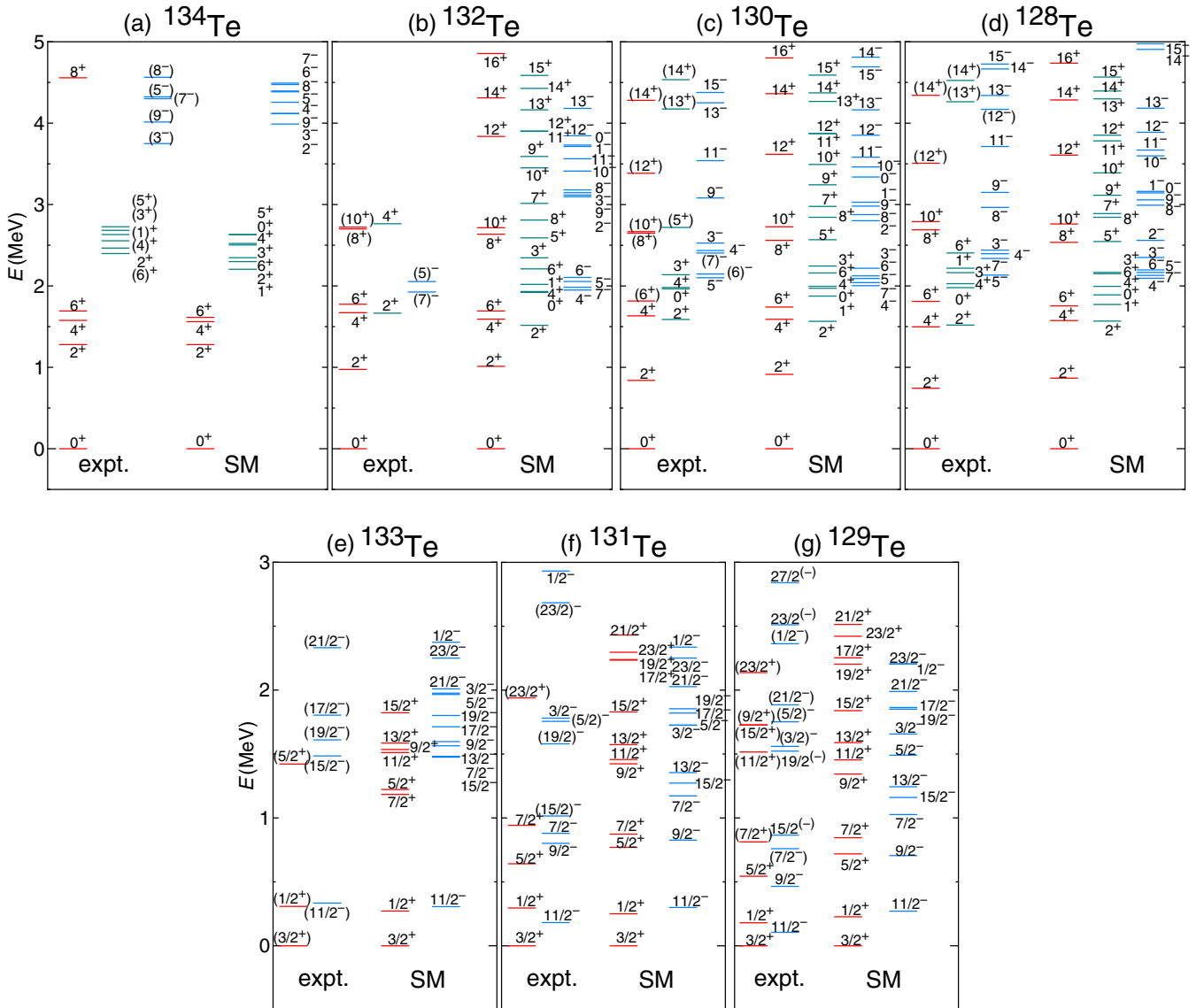


FIG. 4. (Color online) Comparison between the experimental spectra (expt.) and the SM results (SM) for Te isotopes. The experimental data are taken from Refs. [23–25,29,39,40,48–53].

$9/2_1^+$ state was predicted at 1.27 MeV [54]. Their results are consistent with ours.

Table VII shows the theoretical $B(E2)$ values of Te isotopes among the low-lying states in comparison with the experimental data [23,25,29,39,40,48,49,55–59]. Almost all transition rates are well reproduced except for the $B(E2; 10_1^+ \rightarrow 8_1^+)$ value in ^{128}Te . The calculated value is 7.4 times smaller than the experimental value.

The 4_1^+ and 6_1^+ states in ^{134}Te are isomers with half-lives of 1.36(11) ns and 164.1(9) ns [49], respectively. These states are isomers even though the corresponding $B(E2)$ values are not so small. They become isomers since the energy gaps between the initial and final states are small (see Fig. 4).

Table VIII shows the theoretical magnetic dipole moments μ and electric quadrupole moments Q of Te isotopes in comparison with the experimental data [23–25,29,34,35,39,40,48,49,55–59]. Most of the data are well

reproduced. The theoretical magnetic moment of the $3/2_1^+$ state in ^{129}Te agrees with the experimental one, but the theoretical quadrupole moment of the same state is 3.7 times larger than the experimental value. A large discrepancy between experiment and theory is seen in the quadrupole moment of the 2_1^+ state in ^{130}Te although this value has a large experimental error.

4. I isotopes

Here $^{129-135}_{53}\text{I}$ isotopes are discussed. Figure 5 shows the theoretical spectra for I isotopes in comparison with the experimental data [24,25,29,39,40,48,49,60,61]. Energies of the low-lying states in odd-mass nuclei are well reproduced, but energies of their high-spin states are not well reproduced. In particular, differences in energy between experiment and theory for high-spin negative-parity states are large. Further

TABLE VII. Comparison between the experimental $B(E2)$ values (expt.) and the theoretical results (SM) for Te isotopes (in W.u.). The experimental data are taken from Refs. [23,25,29,39,40,48,49,52,55–59].

^{128}Te	Expt.	SM
$2_1^+ \rightarrow 0_1^+$	19.62(18)	21.4
$4_1^+ \rightarrow 2_1^+$		26.7
$6_1^+ \rightarrow 4_1^+$	9.7(6)	11.9
$8_1^+ \rightarrow 6_1^+$		0.171
$10_1^+ \rightarrow 8_1^+$	1.40(12)	0.188
^{129}Te	Expt.	SM
$1/2_1^+ \rightarrow 3/2_1^+$		10.2
$5/2_1^+ \rightarrow 3/2_1^+$		15.2
$5/2_1^+ \rightarrow 1/2_1^+$		0.292
$9/2_1^- \rightarrow 11/2_1^-$		20.2
$7/2_1^- \rightarrow 9/2_1^-$		1.86
$7/2_1^- \rightarrow 11/2_1^-$		14.7
^{130}Te	Expt.	SM
$2_1^+ \rightarrow 0_1^+$	15.1(3)	13.9
$4_1^+ \rightarrow 2_1^+$		14.9
$6_1^+ \rightarrow 4_1^+$	6.1(3)	9.00
$8_1^+ \rightarrow 6_1^+$		0.0516
$10_1^+ \rightarrow 8_1^+$	2.2(1)	0.823
^{131}Te	Expt.	SM
$1/2_1^+ \rightarrow 3/2_1^+$		8.23
$5/2_1^+ \rightarrow 3/2_1^+$		7.92
$5/2_1^+ \rightarrow 1/2_1^+$		0.0212
$9/2_1^- \rightarrow 11/2_1^-$		8.99
$7/2_1^- \rightarrow 9/2_1^-$		1.25
$7/2_1^- \rightarrow 11/2_1^-$		7.83
$17/2_1^- \rightarrow 13/2_1^-$	3.5(10)	3.07
^{132}Te	Expt.	SM
$2_1^+ \rightarrow 0_1^+$	10(1)	7.68
$4_1^+ \rightarrow 2_1^+$		6.90
$6_1^+ \rightarrow 4_1^+$	3.3(2)	5.49
$8_1^+ \rightarrow 6_1^+$		0.0696
$10_1^+ \rightarrow 8_1^+$	1.05(3)	1.10
^{133}Te	Expt.	SM
$1/2_1^+ \rightarrow 3/2_1^+$		5.53
$5/2_1^+ \rightarrow 3/2_1^+$		2.59
$5/2_1^+ \rightarrow 1/2_1^+$		3.62
$19/2_1^- \rightarrow 15/2_1^-$	2.56(14)	2.26
^{134}Te	Expt.	SM
$2_1^+ \rightarrow 0_1^+$	6.3(20)	4.25
$4_1^+ \rightarrow 2_1^+$	4.3(4)	4.96
$6_1^+ \rightarrow 4_1^+$	2.05(4)	2.81
$8_1^+ \rightarrow 6_1^+$		<0.001
$10_1^+ \rightarrow 8_1^+$		1.46

discrepancies between experiment and theory are seen for doubly-odd nuclei to be discussed for each nucleus separately.

^{135}I is a single-closed nucleus with three valence protons. The present results well explain those measured experimental energies of the low-lying positive-parity states. The calculated $11/2_1^-$ state at 2.39 MeV, which mainly consists of the $(\pi g_{7/2}^2 h_{11/2})$ configuration, is not experimentally observed at

TABLE VIII. Comparison of the magnetic dipole moments μ (in μ_N) and the electric quadrupole moments Q (in eb) obtained by the shell model (SM) to the experimental data (expt.) for Te isotopes. The experimental data are taken from Refs. [23–25,29,34,35,39,40,48,49,55–59].

^{128}Te	μ		Q	
	Expt.	SM	Expt.	SM
2_1^+	+0.50(6)	+0.256	-0.06(5)	+0.0288
4_1^+		+1.64		-0.234
6_1^+		+4.64		-0.974
^{129}Te	Expt.	SM	Expt.	SM
$3/2_1^+$	0.702(4)	+0.837	0.055(13)	+0.202
$5/2_1^+$		+0.410		-0.140
$7/2_1^+$		+0.897		-0.0309
$11/2_1^-$	-1.091(7)	-1.29	+0.40(3)	+0.210
^{130}Te	Expt.	SM	Expt.	SM
2_1^+	+0.58(10)	+0.291	-0.15(10)	-0.0262
4_1^+		+2.06		-0.191
6_1^+		+4.27		-0.726
^{131}Te	Expt.	SM	Expt.	SM
$3/2_1^+$	0.696(9)	+0.843		+0.189
$5/2_1^+$		+0.356		-0.130
$7/2_1^+$		+0.835		-0.0434
$7/2_1^-$		-1.39		+0.237
$9/2_1^-$		-1.11		+0.526
$11/2_1^-$	(-)1.04(4)	-1.30	+0.25(14)	+0.319
^{132}Te	Expt.	SM	Expt.	SM
2_1^+	+0.6(3)	+0.350		-0.0367
4_1^+		+2.43		-0.121
6_1^+	+4.7(5)	+4.08		-0.523
^{133}Te	Expt.	SM	Expt.	SM
$3/2_1^+$	+0.85(2)	+0.849	+0.23(9)	+0.154
$5/2_1^+$		+0.626		+0.181
$11/2_1^-$	(-)1.129(7)	-1.31	0.28(14)	+0.363
^{134}Te	expt.	SM	expt.	SM
2_1^+		+1.35		+0.169
4_1^+	3(2)	+2.71		-0.0296
6_1^+	+5.08(15)	+4.10		-0.395

present. The energy of this state was also predicted at around 2.0 MeV in a SM calculation [62].

In ^{133}I , experimental first $11/2_1^-$ state at 2.60 MeV is over 0.8 MeV higher than the theoretical $11/2_1^-$ state. This experimental state may not be the first $11/2_1^-$ state. In fact, several states that might have the spin-parity assignment of $11/2_1^-$ are observed below this state at 2.60 MeV [48]. In this calculation more than ten $11/2_1^-$ states are predicted above the $11/2_1^-$ state below 2.6 MeV. A similar situation applies for the $1/2_1^+$ state. The experimental $1/2_1^+$ state at 2.04 MeV might correspond to the theoretical $1/2_3^+$ state at 1.98 MeV (not shown in the figure).

The $19/2_1^-$ state at 1.63 MeV should be a spin-gap isomer, considering its long half-life of 9(2) s [48]. This indicates that $15/2_1^-$ and $17/2_1^-$ states should appear higher than the $19/2_1^-$ state, but in the present calculation former states are calculated

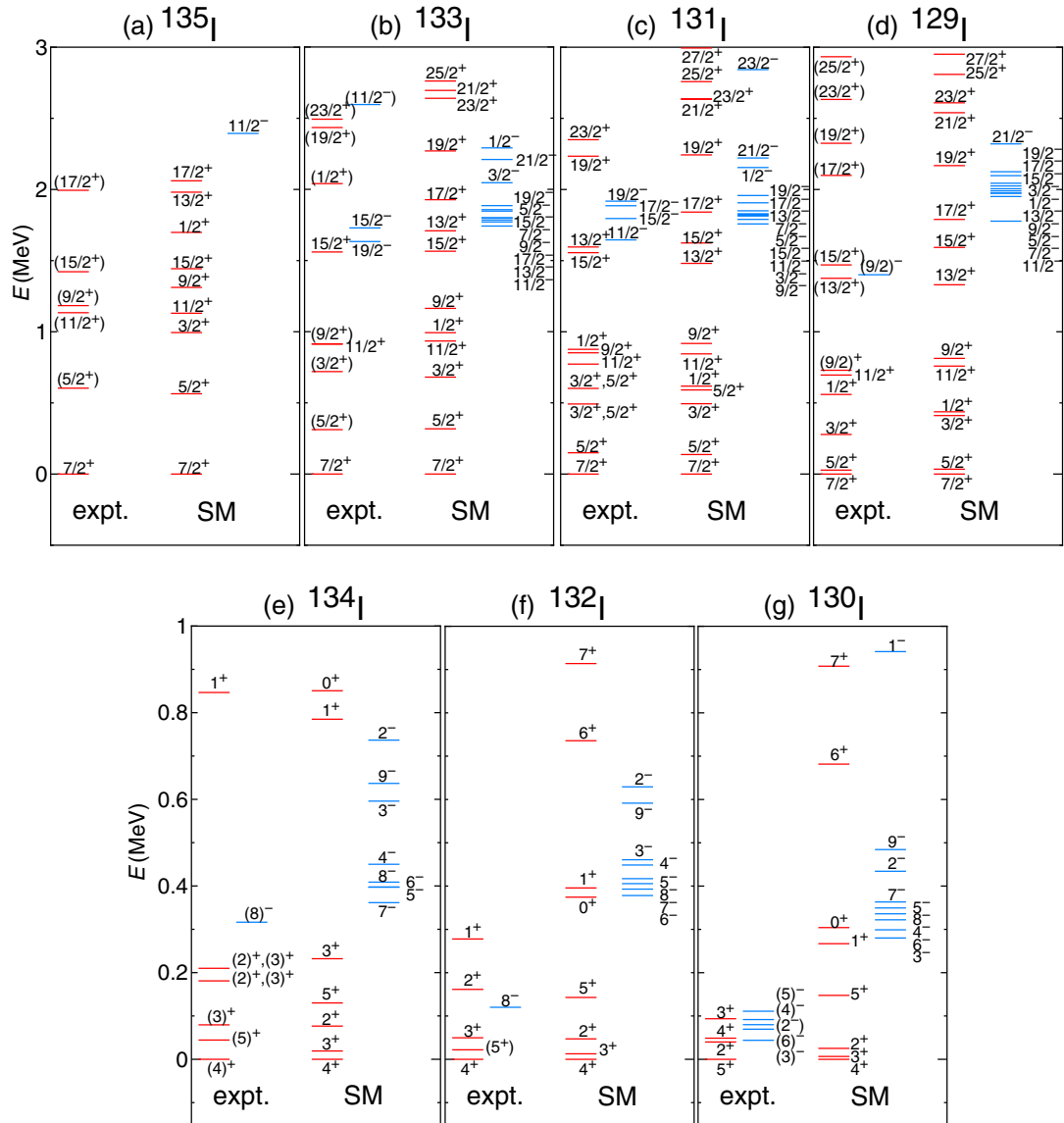


TABLE IX. Comparison between the experimental $B(E2)$ values (expt.) and the theoretical results (SM) for I isotopes (in W.u.). The experimental data are taken from Refs. [24,29,40,49].

^{129}I	Expt.	SM
$3/2_1^+ \rightarrow 5/2_1^+$	13(6)	8.63
$3/2_1^+ \rightarrow 7/2_1^+$	47(6)	30.4
$5/2_1^+ \rightarrow 7/2_1^+$	24(3)	11.1
^{130}I	Expt.	SM
$4_1^+ \rightarrow 3_1^+$		0.372
$2_1^+ \rightarrow 3_1^+$		0.666
$4_1^+ \rightarrow 5_1^+$		15.1
^{131}I	Expt.	SM
$5/2_1^+ \rightarrow 7/2_1^+$		9.13
$3/2_1^+ \rightarrow 7/2_1^+$		23.1
$3/2_1^+ \rightarrow 5/2_1^+$		7.40
^{132}I	Expt.	SM
$2_1^+ \rightarrow 3_1^+$	34(9)	0.00025
$2_1^+ \rightarrow 3_2^+$		6.45
$1_1^+ \rightarrow 2_1^+$	2.4(6)	2.43
$1_1^+ \rightarrow 3_1^+$	14.2(5)	18.3
^{133}I	Expt.	SM
$5/2_1^+ \rightarrow 7/2_1^+$		6.06
$3/2_1^+ \rightarrow 7/2_1^+$		13.5
$3/2_1^+ \rightarrow 5/2_1^+$		4.64
^{134}I	Expt.	SM
$3_1^+ \rightarrow 4_1^+$	15(13)	0.578
$3_2^+ \rightarrow 4_1^+$		3.93
$2_1^+ \rightarrow 3_1^+$		0.169
$5_1^+ \rightarrow 4_1^+$		4.26
^{135}I	Expt.	SM
$5/2_1^+ \rightarrow 7/2_1^+$		3.30
$3/2_1^+ \rightarrow 7/2_1^+$		6.49
$3/2_1^+ \rightarrow 5/2_1^+$		1.95

are known at present. Most of them are well reproduced, but two of them are not reproduced at all. The $B(E2; 2_1^+ \rightarrow 3_1^+)$ value for ^{132}I has the largest discrepancy between experiment [34(9) W.u.] and theory (0.00025 W.u.). This large discrepancy between experiment and theory might be explained by the admixture of related two initial and final states which are closely located in energy. In fact, the 2_1^+ and 2_2^+ states are calculated at 0.047 and 0.275 MeV, respectively. Also the 3_1^+ and 3_2^+ states are calculated at 0.013 and 0.119 MeV, respectively. Regarding the $B(E2; 3_1^+ \rightarrow 4_1^+)$ value in ^{134}I , the theoretical result is 26 times smaller than the experimental one, although this value has a large experimental error. This discrepancy might also be explained by the admixture of related states.

Table X shows the theoretical magnetic dipole moments μ and electric quadrupole moments Q of I isotopes in comparison with the experimental data [24,25,29,35,39,40,48,60]. On the whole, the measured magnetic moments and quadrupole moments are well reproduced by the present calculation. The largest discrepancy is seen in the quadrupole moment for the 4_1^+ state of ^{132}I and the calculated result is 2.8 times larger than the experimental one.

TABLE X. Comparison of the magnetic dipole moments μ (in μ_N) and the electric quadrupole moments Q (in eb) obtained by the shell model (SM) to the experimental data (expt.) for I isotopes. The experimental data are taken from Refs. [24,25,29,35,39,40,48,60].

^{129}I	μ		Q	
	Expt.	SM	Expt.	SM
$3/2_1^+$		+1.25		+0.343
$5/2_1^+$	+2.8045(26)	+3.26	-0.604(10)	-0.726
$7/2_1^+$	+2.6210(3)	+2.25	-0.488(8)	-0.534
^{130}I	Expt.	SM	Expt.	SM
2_1^+		+2.28		-0.481
3_1^+		+2.06		-0.551
4_1^+		+2.48		-0.305
5_1^+	3.349(7)	+2.99		-0.293
^{131}I	Expt.	SM	Expt.	SM
$3/2_1^+$		+1.29		+0.299
$5/2_1^+$	+2.8(5)	+3.28		-0.618
$7/2_1^+$	+2.742(1)	+2.28	-0.35(2)	-0.398
^{132}I	Expt.	SM	Expt.	SM
2_1^+		+1.95		-0.389
3_1^+	+2.24(30)	+1.97	0.20(7)	-0.399
4_1^+	3.088(7)	+2.55	0.08(1)	-0.221
5_1^+		+3.05		-0.169
^{133}I	Expt.	SM	Expt.	SM
$3/2_1^+$		+1.31		+0.233
$5/2_1^+$		+3.36		-0.474
$7/2_1^+$	+2.856(5)	+2.33	-0.24(1)	-0.266
^{134}I	Expt.	SM	Expt.	SM
2_1^+		+1.74		-0.238
3_1^+		+2.01		-0.272
4_1^+		+2.62		-0.145
5_1^+		+3.17		-0.0697
^{135}I	Expt.	SM	Expt.	SM
$3/2_1^+$		+1.02		+0.231
$5/2_1^+$		+3.59		-0.369
$7/2_1^+$	(+2.940(2))	+2.37		-0.175

5. Xe isotopes

Here $^{130-136}_{54}\text{Xe}$ isotopes are discussed. Figure 6 shows the theoretical spectra for Xe isotopes compared to the experimental data [25,29,39,40,48,49,56,60,66,67].

^{136}Xe is a single-closed nucleus with four valence protons. A small energy spacing between 4_1^+ and 6_1^+ states and a large energy spacing between 6_1^+ and 8_1^+ states are reproduced. The 6_1^+ state is an isomer with half-life of 2.95(9) μs [66]. This isomer is analyzed in detail in Sec. III C.

In ^{134}Xe , a small energy spacing between the 8_1^+ and 10_1^+ states is reproduced. There are only three assigned negative-parity states (7_1^- , 9_1^- , and 11_1^- states) below 5 MeV in experiment and these states are well reproduced. They are inferred to have the neutron ($h_{11/2}^{-1}d_{3/2}^{-1}$) configuration with the stretched angular momentum 7, coupled with the proton quadrupole excited states (0^+ , 2^+ , 4^+).

In ^{132}Xe , even-spin yrast states above spin 6 are not assigned except for the 10_1^+ state. The 10_1^+ state is known as an isomer

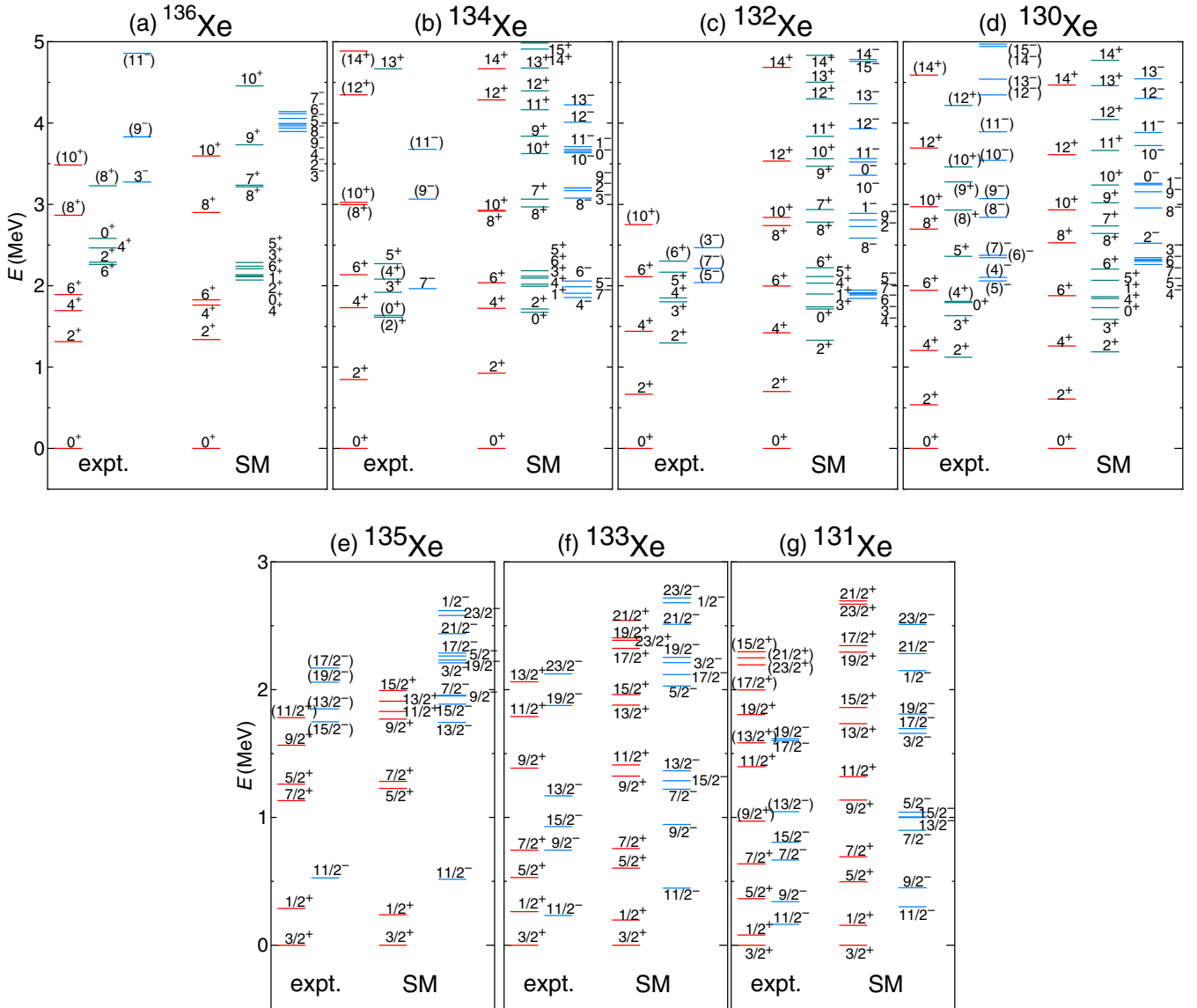


FIG. 6. (Color online) Comparison between the experimental spectra (expt.) and the SM results (SM) for Xe isotopes. The experimental data are taken from Refs. [25,29,39,40,48,49,60,66,74,75].

with long half-life of 8.39(11) ms [40]. Thus it naturally follows that the experimental 8_1^+ and 10_1^+ states are close in energy or the 8_1^+ state is located higher than the 10_1^+ state. However, in the present calculation, the 8_1^+ state is predicted 0.10 MeV lower than the 10_1^+ state. This disagreement can be easily removed by a small modification of interactions, for instance, by a bit change of $G_{8\nu}$ or $G_{10\nu}$ interaction strengths.

The nuclei in the mass region around 130 which have several valence proton particles and valence neutron holes show a characteristic feature known as the γ instability in the low-lying states. This feature originates from the oblate deformation for neutrons and the prolate deformation for protons. The γ instability of the even-even nuclei manifests its appearance in the energy staggering of even-odd spin states (the 2_2^+ , 3_1^+ , 4_2^+ , 5_1^+ , and 6_2^+ states) in the quasi- γ bands and some forbidden transitions between the yrast and the quasi- γ bands [68–70]. The low-lying states of the γ unstable

nuclei were extensively investigated in terms of the interacting boson model (IBM) [68–73], and the energy spectra and the electromagnetic transitions were well approximated by the IBM with the O(6) dynamical symmetry.

In ^{130}Xe , the present calculation well reproduce the energy levels of not only the yrast states up to spin 6 but also the 2_2^+ , 3_1^+ , 4_2^+ , and 5_1^+ states in the quasi- γ band. Concerning the higher spin states, the experimental level spacing between the 8_1^+ and 10_1^+ states is small. On the contrary, the energy spacing between the 10_1^+ and 12_1^+ states becomes large. The present calculation quite well reproduces the behavior of the energy levels for the yrast band. The anomalous behavior at spin 10 is attributed to a band crossing between the S band and the ground band.

In ^{135}Xe , ^{133}Xe , and ^{131}Xe , positive-parity states are well reproduced. In ^{135}Xe , $5/2_1^+$ and $7/2_1^+$ states are reversely predicted, and $13/2_1^-$ and $15/2_1^-$ states are also reversely

TABLE XI. Comparison between the experimental $B(E2)$ values (expt.) and the theoretical results (SM) for Xe isotopes (in W.u.). The experimental data are taken from Refs. [25,29,39,40,49,56,66,67].

^{130}Xe	Expt.	SM
$2_1^+ \rightarrow 0_1^+$	38(5)	41.0
$4_1^+ \rightarrow 2_1^+$	44.5(20)	59.6
$6_1^+ \rightarrow 4_1^+$	>0.033	62.3
$8_1^+ \rightarrow 6_1^+$	>0.020	50.3
$10_1^+ \rightarrow 8_1^+$	1.69(4)	5.99
^{131}Xe	Expt.	SM
$1/2_1^+ \rightarrow 3/2_1^+$	<37	17.9
$5/2_1^+ \rightarrow 1/2_1^+$	7.64(24)	2.30
$5/2_1^+ \rightarrow 3/2_1^+$	27.8(9)	33.3
$7/2_1^+ \rightarrow 3/2_1^+$	22.2(19)	27.6
$7/2_1^- \rightarrow 11/2_1^-$	0.494532(20)	20.8
$7/2_2^- \rightarrow 11/2_1^-$		4.73
$9/2_1^- \rightarrow 11/2_1^-$	39(10)	42.0
^{132}Xe	Expt.	SM
$2_1^+ \rightarrow 0_1^+$	23.1(15)	27.7
$2_2^+ \rightarrow 0_1^+$	0.079(11)	0.000150
$2_2^+ \rightarrow 2_1^+$	41(4)	37.3
$4_1^+ \rightarrow 2_1^+$	28.6(23)	40.4
$6_1^+ \rightarrow 4_1^+$		30.5
$8_1^+ \rightarrow 6_1^+$		17.4
^{133}Xe	Expt.	SM
$1/2_1^+ \rightarrow 3/2_1^+$		15.1
$5/2_1^+ \rightarrow 1/2_1^+$		0.235
$5/2_1^+ \rightarrow 3/2_1^+$		19.9
$7/2_1^+ \rightarrow 3/2_1^+$		17.5
$9/2_1^- \rightarrow 11/2_1^-$		15.2
$15/2_1^- \rightarrow 11/2_1^-$		13.8
^{134}Xe	Expt.	SM
$2_1^+ \rightarrow 0_1^+$	15.3(11)	15.3
$4_1^+ \rightarrow 2_1^+$	11.6(8)	18.6
$6_1^+ \rightarrow 4_1^+$		3.43
$8_1^+ \rightarrow 6_1^+$		4.95
$10_1^+ \rightarrow 8_1^+$	160(50),0.64(1)	0.610
^{135}Xe	Expt.	SM
$1/2_1^+ \rightarrow 3/2_1^+$		9.07
$7/2_1^+ \rightarrow 3/2_1^+$		11.3
$5/2_1^+ \rightarrow 3/2_1^+$		8.24
$5/2_1^+ \rightarrow 1/2_1^+$		4.26
^{136}Xe	Expt.	SM
$2_1^+ \rightarrow 0_1^+$	16.6(24)	8.59
$4_1^+ \rightarrow 2_1^+$	1.281(17)	1.53
$6_1^+ \rightarrow 4_1^+$	0.0132(4)	0.00212
$8_1^+ \rightarrow 6_1^+$		4.08

predicted. However, rough energy positions of these states and energy orderings of other states are reproduced. In ^{133}Xe and ^{131}Xe negative-parity states are 0.1 ~ 0.4 MeV higher than experimental ones. The energies of the negative-parity states depend largely on the single-particle energy of the neutron $h_{11/2}$ orbital. A better fit to these states would be obtained by modifying the single-particle energy.

Table XI shows the theoretical $B(E2)$ values of Xe isotopes among the low-lying states in comparison with the experi-

TABLE XII. Comparison of the magnetic dipole moments μ (in μ) and the electric quadrupole moments Q (in eb) obtained by the shell model (SM) to the experimental data (expt.) for Xe isotopes. The experimental data are taken from Refs. [25,29,35,39,40,48,49,60,66,67].

^{130}Xe	μ		Q	
	Expt.	SM	Expt.	SM
2_1^+	+0.76(14)	+0.611		-0.262
4_1^+	+1.68(20)	+1.50		-0.395
6_1^+		+2.86		-0.508
10_1^+	-2.05(14)	-1.86		+0.452
^{131}Xe	Expt.	SM	Expt.	SM
$3/2_1^+$	+0.691862(4)	+0.892	-0.114(1)	+0.303
$5/2_1^+$		+0.649		-0.249
$7/2_1^-$		-1.34		+0.138
$9/2_1^-$		-1.08		+1.05
$11/2_1^-$	-0.994048(6)	-1.16	+0.73(3)	+0.479
^{132}Xe	Expt.	SM	Expt.	SM
2_1^+	+0.651(24)	+0.622		-0.218
2_2^+	+0.2(4)	+0.563		+0.251
4_1^+	+2.4(4)	+1.85		-0.300
6_1^+		+4.74		-0.517
10_1^+	(-),1.95(5)	-2.28		+1.04
^{133}Xe	Expt.	SM	Expt.	SM
$3/2_1^+$	+0.81340(7)	+0.892	+0.142(5)	+0.293
$5/2_1^+$		+0.651		-0.204
$9/2_1^-$		-1.10		+0.782
$11/2_1^-$	-1.08247(15)	-1.25	+0.77(3)	+0.622
^{134}Xe	Expt.	SM	Expt.	SM
2_1^+	+0.708(14)	+0.647		-0.167
4_1^+	+3.2(6)	+2.22		-0.382
6_1^+		+4.14		-0.268
^{135}Xe	Expt.	SM	Expt.	SM
$3/2_1^+$	+0.9032(7)	+0.889	+0.214(7)	+0.212
$5/2_1^+$		+0.770		+0.109
$7/2_1^+$		+2.46		+0.0795
$11/2_1^-$	-1.1036(14)	-1.27	+0.618(21)	+0.575
^{136}Xe	Expt.	SM	expt.	SM
2_1^+	+1.53(9)	+1.45		-0.0967
4_1^+	3.2(6)	+2.77		-0.0378
6_1^+		+4.07		-0.111

mental data [25,29,39,40,49,56,66,67]. A large discrepancy between experiment and theory is seen in the $B(E2; 7/2_1^- \rightarrow 11/2_1^-)$ value of ^{131}Xe [0.494532(20) W.u. in experiment]. The theoretical $7/2_2^-$ state is predicted to be 0.296 MeV higher than the theoretical $7/2_1^-$ state. Comparing the experimental data with the calculated $B(E2; 7/2_2^- \rightarrow 11/2_1^-)$ value of 4.73 W.u. and the $B(E2; 7/2_1^- \rightarrow 11/2_1^-)$ value of 20.8 W.u., it is inferred that the theoretical $7/2_1^-$ and $7/2_2^-$ states might have been largely admixed. The experimental $B(E2; 2_2^+ \rightarrow 0_1^+)$ value in ^{132}Xe and the $B(E2; 6_1^+ \rightarrow 4_1^+)$ value in ^{136}Xe are very small and the present calculation reproduces this tendency.

Table XII shows the theoretical magnetic dipole moments μ and electric quadrupole moments Q of Xe isotopes in comparison with the experimental

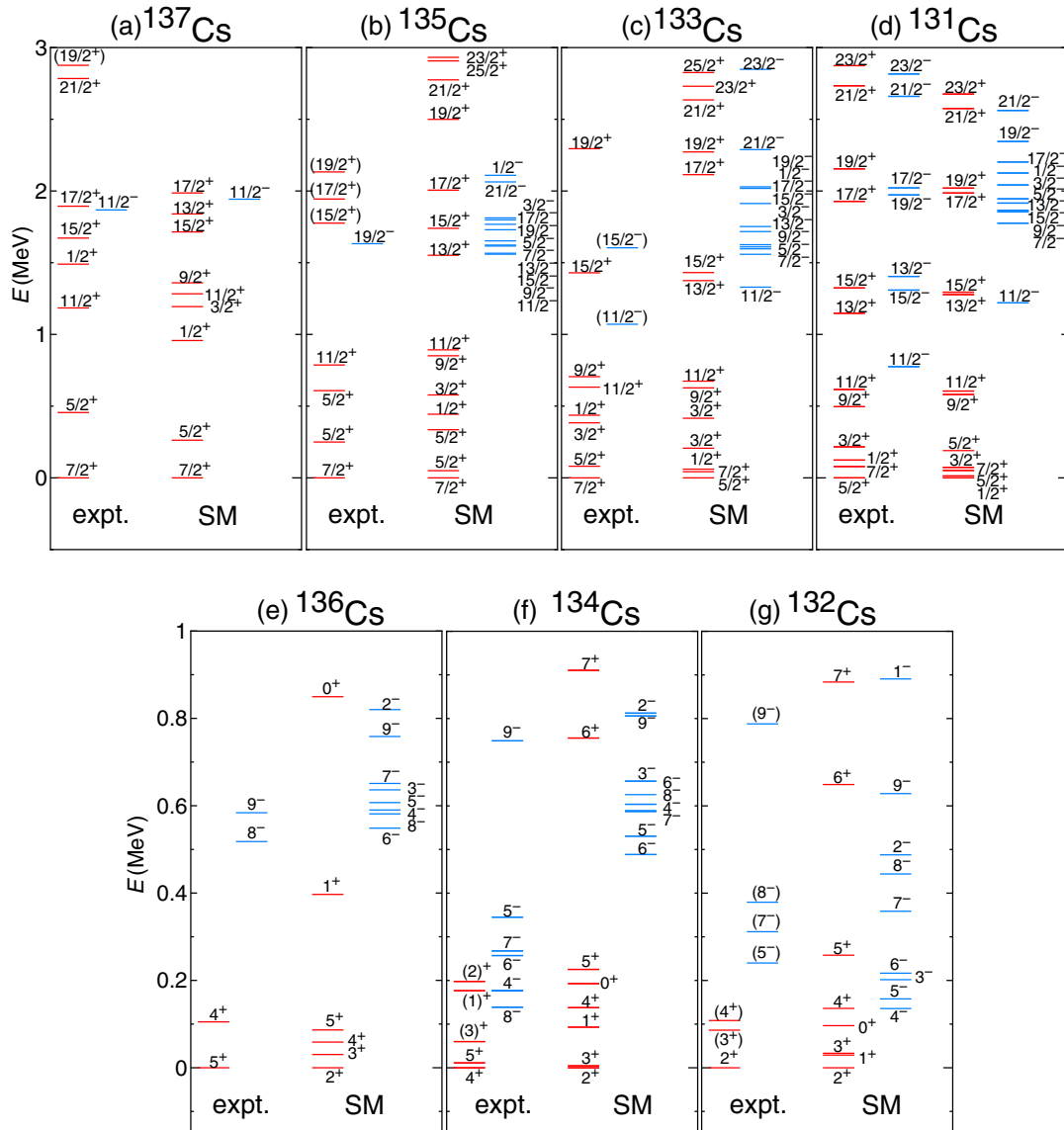


FIG. 7. (Color online) Comparison between the experimental spectra (expt.) and the SM results (SM) for Cs isotopes. The experimental data are taken from Refs. [29,39,40,48,49,60,66,76–79].

data [25,29,35,39,40,48,49,60,66,67]. Theoretical quadrupole moments of all $3/2_1^+$ states in odd-mass Xe isotopes are positive. In experiment, they are also positive except for ^{131}Xe . In all these nuclei, discrepancies between experiment and theory are less than twice and most of the data are reproduced within experimental errors.

6. Cs isotopes

Here $^{131-137}_{55}\text{Cs}$ isotopes are discussed. Figure 7 shows the theoretical spectra for Cs isotopes compared to the experimental data [29,39,40,48,49,60,66,76–79].

^{137}Cs is a single-closed nucleus with five valence protons. The experimental $19/2_1^+$ state at 2.88 MeV and $21/2_1^+$ state at 2.78 MeV are respectively calculated at 3.030 MeV and at 3.032 MeV (not shown in the figure). These two states are found to have the $(\pi g_{7/2}^4 d_{5/2})$ configuration. This is the lowest energy configuration that makes $17/2^+$, $19/2^+$, and

$21/2^+$ states. Theoretically negative-parity states other than the $11/2_1^-$ state are predicted to appear over 3.1 MeV (not shown in the figure).

In ^{135}Cs , the $19/2_1^-$ state at 1.63 MeV is known as a long-lived isomer with a half-life of 53(2) min [60]. By considering its long half-life, this state should be a spin-gap isomer. Therefore, below the $19/2_1^-$ state there should appear no negative-parity states, such as $15/2^-$ and $17/2^-$ states, connected by the $E2$ or $M1$ transitions. However, this situation has not been realized in the present calculation. The detailed analysis is carried out in Sec. III C.

In ^{133}Cs , the spin-parity of the experimental ground state is $7/2^+$. In theory the ordering of the $7/2_1^+$ and $5/2_1^+$ states is reversely predicted although the energy difference between two states is only 0.043 MeV. The ordering of the $11/2_1^+$ and $9/2_1^+$ states is also reversely reproduced with the energy difference of 0.047 MeV.

In ^{131}Cs , the present calculation reproduces the experimental situations such that the $13/2_1^+$ and $15/2_1^+$ states are close in energy and also that the $17/2_1^+$ and $19/2_1^+$ states are close in energy. Negative-parity states are calculated to be about 0.5 MeV higher as a whole.

In odd-mass Cs isotopes such an experimental situation is reproduced such that the energy gaps between the $7/2_1^+$ and $5/2_1^+$ states become smaller as the neutron number decreases and that, finally, the ordering of them is reversed. Also, for the $1/2_1^+$ and $3/2_1^+$ states, our results give the same tendency that their energies become lower as the neutron number decreases. In general negative-parity states are not well reproduced. However, the present calculation reproduces the situation that energy of the $11/2_1^-$ state in each odd-mass Cs isotope goes down as the neutron number decreases.

In ^{136}Cs , the spin-parity of the experimental ground state is 5^+ . However, the theoretical ground state is 2^+ although their energy difference is 0.087 MeV. For the negative-parity levels, only the 8_1^- and 9_1^- states are experimentally observed below 1.0 MeV at present. These two states are members of the $[\nu h_{11/2}^{-1}(\pi g_{7/2}d_{5/2})^5]$ configuration, which makes the $2_1^-, 3_1^-, \dots, 9_1^-$ states. They are calculated to be around 0.5 ~ 0.9 MeV in the present study.

In ^{134}Cs , the spin-parity of the experimental ground state is 4^+ . In contrast, the theoretical ground state is 2^+ although their energy difference is 0.138 MeV. Similarly to other doubly-odd nuclei, e.g., doubly-odd Sb isotopes, $2^-, 3^-, \dots, 9^-$ states made of the configuration with one active neutron hole in the $h_{11/2}$ orbital and one active proton in the $g_{7/2}$ orbital are expected to appear at low energy. The experimental 8_1^- state is too low in energy compared to the neighboring 9_1^- and 7_1^- states. Such a situation is not reproduced. In order to get the 8_1^- state as the lowest negative-parity state and to raise up the 9_1^- state, introduction of multipole interactions might be necessary for the neutron-proton interactions as discussed in Sec. III C for ^{132}Sb .

In ^{132}Cs , unlike other Cs isotopes, the ground state is 2^+ , which is reproduced in the present calculation. The energies of the 3_1^+ and 4_1^+ states are also well reproduced.

Table XIII shows the theoretical $B(E2)$ values of Cs isotopes among the low-lying states in comparison with the experimental data [29,39,48,49,60,77]. In ^{131}Cs , the theoretical $B(E2; 1/2_1^+ \rightarrow 5/2_1^+)$ value agrees with the experimental one. However, neither the $B(E2; 7/2_1^+ \rightarrow 5/2_1^+)$ nor $B(E2; 5/2_2^+ \rightarrow 5/2_1^+)$ values agree with the experimental data. The $5/2_1^+$ and $5/2_2^+$ states are closely located (about 0.18 MeV energy difference) so two states might be mixed due to a slight change of the interactions.

Suppose that the original $5/2_1^+$ and $5/2_2^+$ states are admixed as follows:

$$|\widetilde{5/2_1^+}\rangle = \alpha|5/2_1^+\rangle + \sqrt{1-\alpha^2}|5/2_2^+\rangle, \quad (33)$$

$$|\widetilde{5/2_2^+}\rangle = \sqrt{1-\alpha^2}|5/2_1^+\rangle - \alpha|5/2_2^+\rangle. \quad (34)$$

Here $|\rangle$ represents an eigenstate in Eq. (21) and $|\widetilde{\rangle}$ represents an admixed wave function. If $\alpha = 0.94$ is assumed, the revised transition rates with admixed states are obtained as $B(E2; 7/2_1^+ \rightarrow \widetilde{5/2_1^+}) = 1.20$ W.u. [0.64(24) W.u. in experi-

TABLE XIII. Comparison between the experimental $B(E2)$ values (expt.) and the theoretical results (SM) for Ce isotopes (in W.u.). The experimental data are taken from Refs. [29,39,48,49,60,77].

^{131}Cs	Expt.	SM
$1/2_1^+ \rightarrow 5/2_1^+$	69.5(14)	108
$7/2_1^+ \rightarrow 5/2_1^+$	0.64(24)	11.5
$5/2_2^+ \rightarrow 5/2_1^+$	3.5(3)	0.0793
^{132}Cs	Expt.	SM
$3_1^+ \rightarrow 2_1^+$		29.1
$4_1^+ \rightarrow 3_1^+$		5.09
$4_1^+ \rightarrow 2_1^+$		0.000551
^{133}Cs	Expt.	SM
$5/2_1^+ \rightarrow 7/2_1^+$	5.8(4)	5.34
$3/2_1^+ \rightarrow 7/2_1^+$	12(3)	45.8
$3/2_1^+ \rightarrow 5/2_1^+$	0.04_{-4}^{+7}	3.41
^{134}Cs	Expt.	SM
$3_1^+ \rightarrow 4_1^+$		4.61
$2_1^+ \rightarrow 3_1^+$		23.1
$1_1^+ \rightarrow 2_1^+$		32.9
$1_1^+ \rightarrow 3_1^+$		20.8
$5_1^+ \rightarrow 4_1^+$	4.6(6)	14.6
$6_1^- \rightarrow 8_1^-$	12.9(23)	0.472
$6_2^- \rightarrow 8_1^-$		2.43
^{135}Cs	Expt.	SM
$5/2_1^+ \rightarrow 7/2_1^+$	23(7)	0.229
$5/2_2^+ \rightarrow 7/2_1^+$		28.6
$3/2_1^+ \rightarrow 7/2_1^+$		19.9
$3/2_1^+ \rightarrow 5/2_1^+$		1.61
^{136}Cs	Expt.	SM
$3_1^+ \rightarrow 4_1^+$		0.00176
$2_1^+ \rightarrow 3_1^+$		0.613
$1_1^+ \rightarrow 2_1^+$		1.04
$1_1^+ \rightarrow 3_1^+$		0.0619
^{137}Cs	Expt.	SM
$5/2_1^+ \rightarrow 7/2_1^+$	>6.8	0.0493
$5/2_2^+ \rightarrow 7/2_1^+$		16.4
$3/2_1^+ \rightarrow 7/2_1^+$		8.79
$11/2_1^+ \rightarrow 7/2_1^+$		7.91

ment] and $B(E2; \widetilde{5/2_2^+} \rightarrow \widetilde{5/2_1^+}) = 4.32$ W.u. [3.5(3) W.u. in experiment].

The calculated $B(E2; 6_1^- \rightarrow 8_1^-)$ value for the ^{134}Cs nucleus is nearly 30 times smaller than the experimental one. The energy difference between the 6_1^- and 6_2^- states is 0.14 MeV and a small admixture of wave functions might explain this discrepancy. In fact, the theoretical $B(E2; 6_2^- \rightarrow 8_1^-)$ value is 5.1 times larger than the $B(E2; 6_1^- \rightarrow 8_1^-)$ value.

In ^{135}Cs , the difference of the $B(E2; 5/2_1^+ \rightarrow 7/2_1^+)$ values between experiment and theory is also large. The $5/2_1^+$ and $5/2_2^+$ states are calculated at 0.05 and 0.44 MeV, respectively. Thus the energy difference between these states is tiny. For the $5/2_2^+$ state, the $B(E2; 5/2_2^+ \rightarrow 7/2_1^+)$ value equals 28.6 W.u. Therefore the mixture of the $5/2_1^+$ and $5/2_2^+$ states might cause the large experimental $B(E2; 5/2_1^+ \rightarrow 7/2_1^+)$ value.

Table XIV shows the theoretical magnetic dipole moments μ and electric quadrupole moments Q of

TABLE XIV. Comparison of the magnetic dipole moments μ (in μ_N) and the electric quadrupole moments Q (in eb) obtained by the shell model (SM) to the experimental data (expt.) for Cs isotopes. The experimental data are taken from Refs. [29,34,35,39,40,48,49,60,66,77].

^{131}Cs	μ		Q	
	Expt.	SM	Expt.	SM
$3/2_1^+$		+0.753		+0.367
$5/2_1^+$	+3.543(2)	+2.72	-0.575(6)	-0.867
$5/2_2^+$	+1.86(8)	+2.02	0.022(2)	-0.175
$7/2_1^+$		+2.04		-0.423
$11/2_1^-$	6.3(9)	+6.61		-1.65
^{132}Cs	Expt.	SM	Expt.	SM
2_1^+	+2.222(7)	+2.31	+0.508(7)	+0.112
3_1^+		+2.70		-0.535
4_1^+		+2.35		-0.0383
5_1^+		+2.99		-0.272
^{133}Cs	Expt.	SM	Expt.	SM
$3/2_1^+$		+0.725		+0.234
$3/2_2^+$		+1.09		-0.179
$5/2_1^+$	+3.45(2)	+3.14	-0.33(2)	-0.729
$5/2_2^+$	+2.0(2)	+1.92		-0.0925
$7/2_1^+$	+2.582025(3)	+2.20	-0.00371(14)	-0.284
^{134}Cs	Expt.	SM	Expt.	SM
2_1^+		+2.49		-0.125
3_1^+		+3.01		-0.470
4_1^+	+2.9937(9)	+2.64	+0.389(3)	+0.0248
5_1^+	+3.35(7)	+3.11		-0.0627
8_1^-	+1.0978(2)	+0.751	+0.98(8)	+0.742
^{135}Cs	Expt.	SM	Expt.	SM
$3/2_1^+$		+0.800		+0.0357
$5/2_1^+$		+3.63		-0.541
$7/2_1^+$	+2.7324(2)	+2.33	+0.050(2)	-0.104
$19/2_1^-$	+2.18(1)	+1.68	+0.89(7)	+0.943
^{136}Cs	Expt.	SM	Expt.	SM
2_1^+		+1.52		-0.116
3_1^+		+1.98		-0.222
4_1^+		+2.70		+0.0633
5_1^+	+3.711(15)	+3.28	+0.225(10)	+0.128
8_1^-	+1.319(7)	+0.755	+0.74(10)	+0.663
^{137}Cs	Expt.	SM	expt.	SM
$3/2_1^+$		+0.841		-0.0454
$5/2_1^+$		+3.89		-0.386
$7/2_1^+$	+2.8413(1)	+2.38	+0.051(1)	-0.00617

Cs isotopes in comparison with the experimental data [29,34,35,39,40,48,49,60,66,77]. Almost all data are well reproduced except for the following two cases. The experimental quadrupole moment of the $7/2_1^+$ state in ^{133}Cs is too small [-0.00371(14) eb] to be reproduced in theory (-0.284 eb). The theoretical quadrupole moment of the 4_1^+ state in ^{134}Cs (+0.0248 eb) is much smaller than the experimental one [+0.389(3) eb].

7. Ba isotopes

Here $^{132-138}_{56}\text{Ba}$ isotopes are discussed. Figure 8 shows the theoretical spectra for Ba isotopes in comparison with the experimental data [9,29,40,48,49,60,66,77,80–83].

One feature of energy spectra in even-even Ba isotopes is seen in the small energy spacing between 8_1^+ and 10_1^+ states. The present calculation well reproduces this experimental situation except for ^{132}Ba .

In ^{138}Ba , the experimental 12_1^+ state at 4.69 MeV is calculated at 5.21 MeV (not shown in the figure). In experiment the negative-parity 3_1^- state appears low in energy (2.88 MeV) compared to other negative-parity states, which is reproduced a little higher in theory (3.73 MeV). In order to lower the energy of the 3_1^- state, introduction of octupole interactions might be necessary, which is not considered in the present scheme.

In ^{134}Ba , the theoretical energy levels of the even-spin yrast states are well reproduced except for the 6_1^+ state, which is lower than the experimental one. The staggering patterns of the energy levels in the quasi- γ band are also described well, indicating the γ instability in the low-lying states. The nucleus ^{132}Ba is one of the best-studied examples of the γ instability, since the energy levels and the electromagnetic transitions display the typical features of the O(6) dynamical symmetry of the IBM [68–70]. Concerning the low-lying states, a qualitative agreement between theoretical energy levels and experimental ones is clearly seen. In particular, the even-odd staggering in the quasi- γ band is well reproduced. For higher energy states, the experimental energy spacing between 8_1^+ and 10_1^+ states is small. In contrast, the theoretical energy spacing is larger. Apparently modification of two-body interactions is necessary in order to reproduce the experimental situation.

Concerning Ba odd-mass nuclei, energies of the positive-parity yrast states are well reproduced. There exist some discrepancies between the experimental spectra and theoretical ones for negative-parity states.

In ^{133}Ba , the spin-parity of the experimental ground state is $1/2^+$, but the theoretical $1/2_1^+$ state is slightly higher (0.061 MeV) than the $3/2_1^+$ state, which is the ground state in theory. The $9/2_1^-$ state is predicted to be the lowest negative-parity state. The $9/2_1^-$ state is not observed at present. In theory, the $9/2_1^-$ state becomes lower and lower in energy as the neutron number decreases for the odd-mass Ba isotopes. In fact, the $9/2_1^-$ state is experimentally the lowest negative-parity state in ^{131}Ba (0.188 MeV).

Table XV shows the theoretical $B(E2)$ values of Ba isotopes among low-lying states in comparison with the experimental data [29,40,48,49,60,66,77,80,82]. The $B(E2)$ values among yrast states become larger and larger from ^{136}Ba to ^{132}Ba since the contribution to the $B(E2)$ values from the neutron collective motion increases as the neutron-hole number increases.

The $B(E2; I \rightarrow I-2)$ values ($I=2,4,6,8$) among the yrast states in each even-even Ba isotope are several score the Weisskopf estimate. This is mainly due to collective motion for the proton part. In contrast, $B(E2; 10_1^+ \rightarrow 8_1^+)$ values are much smaller compared to other $E2$ transitions. As a result of these small $B(E2)$ values, the 10_1^+ states become isomers, also partly because the energy spacings between the 10_1^+ and 8_1^+ states are small.

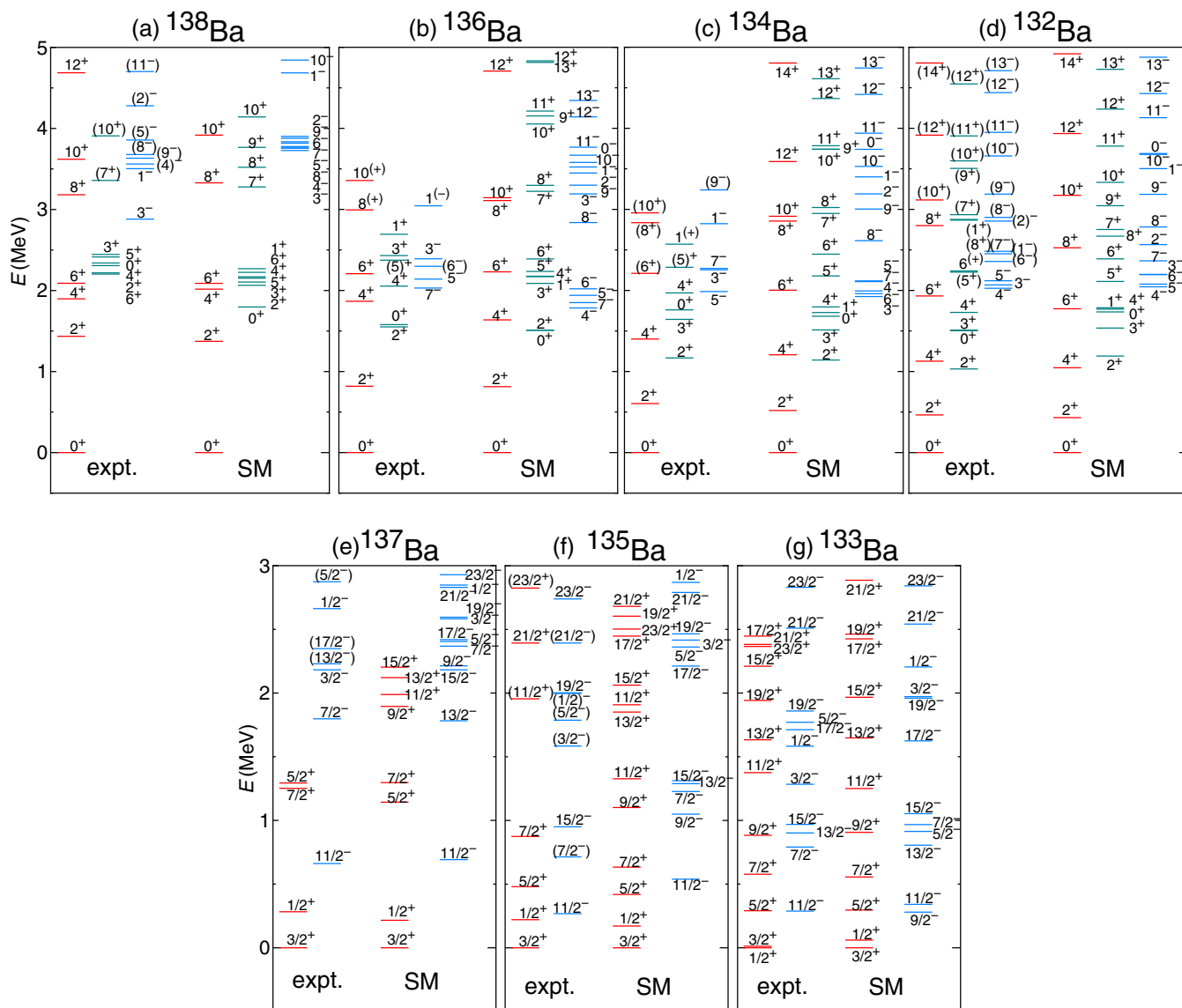


FIG. 8. (Color online) Comparison between the experimental spectra (expt.) and the SM results (SM) for Ba isotopes. The experimental data are taken from Refs. [9,29,40,48,49,60,66,77,80–83].

In ^{132}Ba , the calculated $B(E2; 10_1^+ \rightarrow 8_1^+)$ value is not so small, which is contradictory to the experimental situation. In order to reproduce this small $B(E2; 10_1^+ \rightarrow 8_1^+)$ value, large modification of the wave functions of the 8_1^+ and/or 10_1^+ states is necessary. In fact, as mentioned earlier, the experimental small energy spacing between the 8_1^+ and 10_1^+ states is not so well reproduced in theory.

A large discrepancy between experiment and theory is seen for the $B(E2; 6_1^+ \rightarrow 4_1^+)$ value (13.3 W.u. in theory) in ^{136}Ba . The 6_2^+ state is located 0.16 MeV higher than the 6_1^+ state in the calculation, and the theoretical $B(E2; 6_2^+ \rightarrow 4_1^+)$ value (1.66 W.u.) is near the experimental $B(E2; 6_1^+ \rightarrow 4_1^+)$ value [0.574(25) W.u.]. Thus it is inferred that wave functions of the 6_1^+ and 6_2^+ states are largely admixed.

Table XVI shows the theoretical magnetic dipole moments μ and electric quadrupole moments Q of Ba isotopes in comparison with the experimental

data [29,34,35,40,48,49,60,66,77,80]. The present calculation well reproduces the experimental data.

8. $M1$ transitions

Table XVII shows the comparison between experimental and theoretical $B(M1)$ values [25,29,39,40,48,49,60,66,80,84,85] for Sn, Sb, Te, I, Xe, Cs, and Ba isotopes. The experimentally measured $B(M1)$ values and some $B(M1; 2_i^+ \rightarrow 2_1^+)$ values for even-even nuclei are mainly shown. Most of the experimental transitions are very small and well reproduced in theory. However, in some nuclei the present results differ from the experimental data by a few orders of magnitude.

$M1$ transition rates for even-even nuclei have been studied from the viewpoint of mixed symmetries [86–89]. Experimental $B(M1; 2_3^+ \rightarrow 2_1^+)$ values are much larger than the experimental $B(M1; 2_2^+ \rightarrow 2_1^+)$ values in ^{132}Xe and ^{134}Xe .

TABLE XV. Comparison between the experimental $B(E2)$ values (expt.) and the theoretical results (SM) for Ba isotopes (in W.u.). The experimental data are taken from Refs. [29,40,48,49,60,66,77,80,82].

^{132}Ba	Expt.	SM
$2_1^+ \rightarrow 0_1^+$	43(4)	53.1
$2_2^+ \rightarrow 0_1^+$	3.9(4)	1.80
$4_1^+ \rightarrow 2_1^+$		76.9
$6_1^+ \rightarrow 4_1^+$		81.3
$8_1^+ \rightarrow 6_1^+$		77.0
$10_1^+ \rightarrow 8_1^+$	0.462(10)	21.9
^{133}Ba	Expt.	SM
$3/2_1^+ \rightarrow 1/2_1^+$	<18	9.83
$5/2_1^+ \rightarrow 1/2_1^+$		10.7
$5/2_1^+ \rightarrow 3/2_1^+$		54.1
^{134}Ba	Expt.	SM
$2_1^+ \rightarrow 0_1^+$	33.6(6)	38.8
$2_2^+ \rightarrow 0_1^+$	0.42(13)	0.439
$2_2^+ \rightarrow 2_1^+$	73(22)	21.4
$4_1^+ \rightarrow 2_1^+$	52(6)	57.5
$6_1^+ \rightarrow 4_1^+$		60.9
$8_1^+ \rightarrow 6_1^+$		54.5
$10_1^+ \rightarrow 8_1^+$	0.102(6)	0.522
^{135}Ba	Expt.	SM
$1/2_1^+ \rightarrow 3/2_1^+$	4.6(2)	16.2
$1/2_2^+ \rightarrow 3/2_1^+$	11.7(10)	2.21
$3/2_2^+ \rightarrow 3/2_1^+$	18.0(10)	10.9
$5/2_1^+ \rightarrow 1/2_1^+$	2.6(5)	1.31
$5/2_1^+ \rightarrow 3/2_1^+$	28.3(10)	37.2
$7/2_1^+ \rightarrow 3/2_1^+$	19.9(8)	25.0
^{136}Ba	Expt.	SM
$2_1^+ \rightarrow 0_1^+$	19.87 $^{+54}_{-53}$	22.7
$2_2^+ \rightarrow 0_1^+$	0.78(19)	0.0158
$2_2^+ \rightarrow 2_1^+$	15(4)	19.9
$4_1^+ \rightarrow 2_1^+$		31.2
$6_1^+ \rightarrow 4_1^+$	0.574(25)	13.3
$6_2^+ \rightarrow 4_1^+$		1.66
$8_1^+ \rightarrow 6_1^+$		26.1
$10_1^+ \rightarrow 8_1^+$	0.023(2)	0.0435
^{137}Ba	Expt.	SM
$1/2_1^+ \rightarrow 3/2_1^+$		11.7
$5/2_1^+ \rightarrow 1/2_1^+$		0.888
$5/2_1^+ \rightarrow 3/2_1^+$		17.7
$7/2_1^+ \rightarrow 3/2_1^+$	12.5(11)	16.3
^{138}Ba	Expt.	SM
$2_1^+ \rightarrow 0_1^+$	10.8(5)	12.8
$2_2^+ \rightarrow 0_1^+$	2.01(20)	0.120
$4_1^+ \rightarrow 2_1^+$	0.2873(15)	0.581
$6_1^+ \rightarrow 4_1^+$	0.053(7)	0.628
$8_1^+ \rightarrow 6_1^+$	0.32 $^{+23}_{-4}$	3.30
$10_1^+ \rightarrow 8_1^+$	1.59(22)	3.04

The present work reproduces these situations. The 2_3^+ states in ^{132}Xe and ^{134}Xe have a mixed symmetric nature. The $B(M1; 2_i^+ \rightarrow 2_j^+)$ values of these nuclei were also calculated in Ref. [87] using the SM. Their calculations gave similar results to ours.

TABLE XVI. Comparison of the magnetic dipole moments μ (in μ_N) and the electric quadrupole moments Q (in eb) obtained by the SM (SM) to the experimental data (expt.) for Ba isotopes. The experimental data are taken from Refs. [29,34,35,40,48,49,60,66,77,80].

^{132}Ba	μ		Q	
	Expt.	SM	Expt.	SM
2_1^+	+0.68(6)	+0.801		-0.822
4_1^+		+1.55		-1.06
6_1^+		+1.77		-1.12
10_1^+	-1.59(5)	-1.25		+0.298
^{133}Ba	Expt.	SM	Expt.	SM
$3/2_1^+$	+0.58(8)	+0.928		+0.321
$5/2_1^+$		+0.797		-0.363
$7/2_1^-$		+1.71		-0.668
$11/2_1^-$	0.91(5)	-0.925	+0.89(7)	+0.715
^{134}Ba	Expt.	SM	Expt.	SM
2_1^+	+0.84(10)	+0.855	-0.26(8)	-0.646
4_1^+		+1.89		-0.839
6_1^+		+2.83		-0.827
10_1^+	-2.0(1)	-2.23		1.61
^{135}Ba	Expt.	SM	Expt.	SM
$3/2_1^+$	+0.837943(17)	+0.921	+0.160(3)	+0.395
$5/2_1^+$		+0.991		-0.272
$7/2_1^+$		+1.53		-0.429
$11/2_1^-$	-1.001(15)	-1.17	+0.96(8)	+1.02
^{136}Ba	Expt.	SM	Expt.	SM
2_1^+	+0.69(10)	+0.986	-0.19(6)	-0.387
4_1^+		+2.48		-0.765
6_1^+		+4.40		-0.262
^{137}Ba	Expt.	SM	Expt.	SM
$3/2_1^+$	+0.937365(20)	+0.927	+0.245(4)	+0.258
$5/2_1^+$		+1.50		-0.0559
$7/2_1^+$		+2.72		-0.167
$11/2_1^-$	-0.992(26)	-1.21	+0.78(9)	+0.816
^{138}Ba	Expt.	SM	Expt.	SM
2_1^+	+1.4(2)	+1.71	-0.14(7)	-0.320
4_1^+	+3.2(6)	+2.87		-0.0866
6_1^+	+5.86(12)	+4.16		+0.132

For even-even nuclei of Te and Ba isotopes, large $M1$ transition rates are measured from the third (^{136}Ba) or fourth (^{128}Te , ^{130}Te , and ^{134}Ba) 2^+ state to the first 2^+ state. In these nuclei, however, the third and fourth 2^+ states are close together in theory and there is some possibility that they might have been inversely reproduced.

C. Detailed description of some specific nuclei and isomeric states

In this section we first take up those nuclei which have been essential to determine two-body effective interactions (^{130}Sn , ^{134}Te , and ^{132}Sb). Moreover, the ^{135}Cs nucleus is studied to check the validity of two-body interactions. Next some isomeric states are dealt with to analyze in detail. There are several reasons why states become isomers. Due to their reasons for existence, they are classified as K isomers, spin-gap isomers, shape isomers, and so on [43]. Many isomers in this region are

TABLE XVII. Comparison between the experimental $B(M1)$ values and the theoretical results (SM) for Sn, Sb, Te, I, Xe, Cs, and Ba isotopes (in μ_N^2). The experimental data are taken from Refs. [25,29,39,40,49,60,66,80,84,85].

Nucleus	Transitions	Expt.	SM
^{130}Sn	$4_1^- \rightarrow 5_1^-$	>0.016	0.272
^{132}Sb	$3_1^+ \rightarrow 4_1^+$	$1.12(2) \times 10^{-3}$	4.29×10^{-3}
	$2_1^+ \rightarrow 3_1^+$	0.029(3)	0.0102
	$2_2^+ \rightarrow 2_1^+$	$1.2(10) \times 10^{-3}$	1.12×10^{-2}
	$2_2^+ \rightarrow 3_1^+$	$6(4) \times 10^{-3}$	3.47×10^{-3}
	$1_1^+ \rightarrow 2_1^+$	$>3.4 \times 10^{-4}$	2.45×10^{-3}
^{128}Te	$1_1^+ \rightarrow 2_2^+$	>0.016	0.758
	$2_2^+ \rightarrow 2_1^+$		0.0597
	$2_3^+ \rightarrow 2_1^+$		0.0359
	$2_4^+ \rightarrow 2_1^+$		0.175
^{130}Te	$2_2^+ \rightarrow 2_1^+$		0.148
	$2_3^+ \rightarrow 2_1^+$		0.0167
	$2_4^+ \rightarrow 2_1^+$		0.165
^{132}Te	$2_2^+ \rightarrow 2_1^+$		0.234
	$2_3^+ \rightarrow 2_1^+$		1.61×10^{-5}
^{131}I	$5/2_1^+ \rightarrow 7/2_1^+$	$5.6(3) \times 10^{-3}$	1.39×10^{-3}
^{132}I	$3_1^+ \rightarrow 4_1^+$	$3.74(12) \times 10^{-3}$	$<10^{-5}$
	$3_2^+ \rightarrow 4_1^+$		1.47×10^{-3}
	$2_1^+ \rightarrow 3_1^+$	$1.93(19) \times 10^{-3}$	5.09×10^{-3}
	$1_1^+ \rightarrow 2_1^+$	$1.42(14) \times 10^{-4}$	3.78×10^{-3}
^{134}I	$3_1^+ \rightarrow 4_1^+$	0.0107(8)	1.88×10^{-3}
	$3_2^+ \rightarrow 4_1^+$		8.63×10^{-3}
	$3_1^+ \rightarrow 4_2^+$		0.0503
	$5_1^+ \rightarrow 4_1^+$	$2.80(9) \times 10^{-3}$	1.29×10^{-3}
^{130}Xe	$2_2^+ \rightarrow 2_1^+$		5.31×10^{-3}
	$2_3^+ \rightarrow 2_1^+$		0.233
^{131}Xe	$5/2_1^+ \rightarrow 3/2_1^+$	$3.0(3) \times 10^{-4}$	3.17×10^{-5}
	$3/2_2^+ \rightarrow 3/2_1^+$	$6(6) \times 10^{-3}$	3.45×10^{-4}
^{132}Xe	$2_2^+ \rightarrow 2_1^+$	$1.54(19) \times 10^{-3}$	5.71×10^{-3}
	$2_3^+ \rightarrow 2_1^+$	0.22(6)	0.263
^{134}Xe	$2_2^+ \rightarrow 2_1^+$	0.015(1)	0.0540
	$2_3^+ \rightarrow 2_1^+$	0.30(2)	0.262
^{136}Xe	$6_2^+ \rightarrow 6_1^+$	$>3 \times 10^{-4}$	3.49×10^{-5}
^{133}Cs	$5/2_1^+ \rightarrow 7/2_1^+$	$2.381(22) \times 10^{-3}$	$<10^{-5}$
	$3/2_1^+ \rightarrow 5/2_1^+$	0.011(3)	2.07×10^{-5}
	$1/2_1^+ \rightarrow 3/2_1^+$	>0.024	$<10^{-5}$
^{134}Cs	$5_1^+ \rightarrow 4_1^+$	$3.63(13) \times 10^{-3}$	1.27×10^{-3}
^{135}Cs	$5/2_1^+ \rightarrow 7/2_1^+$	$2.3(7) \times 10^{-3}$	$<10^{-5}$
^{134}Ba	$2_2^+ \rightarrow 2_1^+$		0.0124
	$2_3^+ \rightarrow 2_1^+$		1.29×10^{-3}
	$2_4^+ \rightarrow 2_1^+$		0.357
^{135}Ba	$1/2_1^+ \rightarrow 3/2_1^+$	$2.5(11) \times 10^{-3}$	1.63×10^{-3}
	$5/2_1^+ \rightarrow 3/2_1^+$	$4.2(20) \times 10^{-3}$	5.36×10^{-3}
	$7/2_1^+ \rightarrow 5/2_1^+$	$3.2(3) \times 10^{-3}$	0.0234
^{136}Ba	$2_2^+ \rightarrow 2_1^+$	0.013(4)	0.0316
	$2_3^+ \rightarrow 2_1^+$		0.307
^{138}Ba	$4_2^+ \rightarrow 4_1^+$	0.021(9)	0.0245
	$6_2^+ \rightarrow 6_1^+$	0.15(5)	0.0316
	$5_1^+ \rightarrow 6_2^+$	0.026(14)	0.274

spin-gap isomers, which do not undertake gamma transitions with low-spin change, such as $E2$ or $M1$ transitions, because of the large spin difference between initial and final states. In particular, many of the isomers whose half-lives are longer than few seconds are known to be spin-gap isomers. On the other hand, some states become isomers in spite that these states can be connected to a lower state by low-spin transitions. In this section such isomers are mainly analyzed.

To analyze isomeric states in detail, the PTSM calculations are carried out. The PTSM is one of the shell-model approaches, but a gigantic SM space is restricted to the space mainly made of only low-spin collective pairs. The details of the PTSM are given in Refs. [12–14]. In these papers, angular momenta $L = 0$ (S), $L = 2$ (D), and $L = 4$ (G) collective pairs, and some other noncollective pairs are introduced. The S pair represents

$$S^\dagger = \sum_j \alpha_j A_0^{\dagger(0)}(jj), \quad (35)$$

and D pair and G pair are constructed as

$$D_M^\dagger = \sum_{j_1 j_2} \beta_{j_1 j_2} A_M^{\dagger(2)}(j_1 j_2), \quad (36)$$

$$G_M^\dagger = \sum_{j_1 j_2} \gamma_{j_1 j_2} A_M^{\dagger(4)}(j_1 j_2), \quad (37)$$

where $A_M^{\dagger(J)}(j_1 j_2)$ is the creation operator of the pair of nucleons defined in Eq. (10).

1. ^{130}Sn , ^{134}Te , and ^{132}Sb

Here ^{130}Sn , ^{134}Te , and ^{132}Sb nuclei are analyzed with respect to neutron two-body effective interactions, proton two-body effective interactions, and neutron-proton two-body effective interactions, respectively. Figure 9 shows the theoretical energy spectra in comparison with the experimental data [25,40,49]. All observed and theoretical energy levels are shown below 5.0 MeV for ^{130}Sn and ^{134}Te and those below 1.6 MeV for ^{132}Sb . Here experimental levels without any assignment of spin-parity are also presented in the figure.

^{130}Sn is a single-closed nucleus with two valence neutrons. The present calculation reproduces experimental energy levels well in general. However, energies of the 4_1^+ and 6_1^+ states are not so well reproduced. They would be adjusted to the experimental energies by changing $G_{4\nu}$ and $G_{6\nu}$ strengths.

Some negative-parity states are almost degenerate so it is hard to reproduce the ordering of the low-lying negative-parity states. Through the analysis of the wave functions, the 4_1^- , 5_1^- , 6_1^- , and 7_1^- states bunched at around 2.1 MeV consist of the $(\nu h_{11/2}^{-1} d_{3/2}^{-1})$ configuration. They are experimentally observed at the corresponding energies in theory although the 6_1^- state is not observed. Theoretical 5_2^- and 6_2^- states of the $(\nu h_{11/2}^{-1} s_{1/2}^{-1})$ configuration are both located at 2.46 MeV. Theoretical 3_1^- , 4_2^- , 5_3^- , 6_3^- , 7_2^- , 8_1^- states bunched at around 3.7 MeV are members of the $(\nu h_{11/2}^{-1} d_{5/2}^{-1})$ configuration and 2_1^- , 3_2^- , 4_3^- , 5_4^- , 6_4^- , 7_3^- , 8_2^- , 9_1^- states bunched at around 4.5 MeV are members of the $(\nu h_{11/2}^{-1} g_{7/2}^{-1})$ configuration.

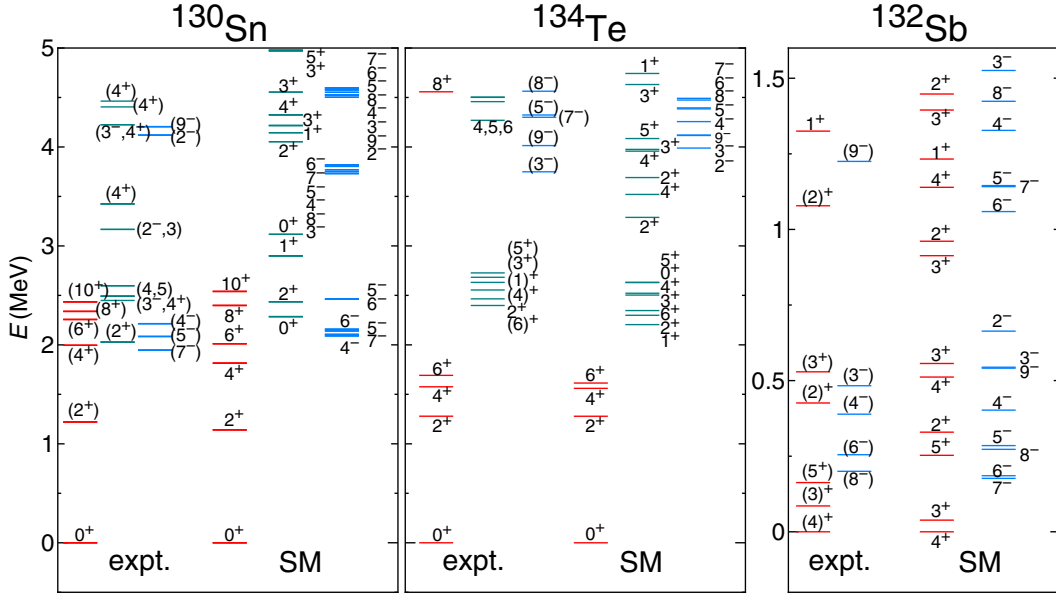


FIG. 9. (Color online) Comparison between the experimental spectra (expt.) and the SM results (SM) for ^{130}Sn , ^{134}Te , and ^{132}Sb . The experimental data are taken from Refs. [25,29,40,49].

^{134}Te is a single-closed nucleus with two valence protons. A prominent feature in experiment for ^{134}Te is the large energy gap between the 6_1^+ and 8_1^+ states. The yrast states up to spin 6 are mainly made of two valence protons in the $g_{7/2}$ orbital. In order to construct a positive-parity state with higher spin more than 6, a neutron in the $h_{11/2}$ orbital should be excited to a higher orbital beyond the magic number 82. Otherwise, two protons in the $g_{7/2}$ orbital should be excited to the $h_{11/2}$ orbital. These excitations need a large amount of energy. Consequently, this feature of large energy spacing arises. In fact theoretical 8_1^+ state is predicted at 7.34 MeV (not shown in the figure) with the $(\pi h_{11/2}^2)$ configuration.

The band starting from the 8^+ state at 4.56 MeV up to the 15^+ at 7.57 MeV (not shown in the figure) is experimentally observed except for the 11^+ state, which is presumed to be a neutron core-excited band. These states are outside the framework of the present model. It is easily understood that any 9^+ state (e.g., experimental level at 5.08 MeV) cannot be constructed by angular-momentum coupling of two-proton states in the framework of the present model space. Theoretical calculations for this core-excited band were performed in Refs. [62,90]. In these papers, it was concluded that this band has the $(\nu f_{7/2} h_{11/2}^{-1} \pi g_{7/2}^2)$ configuration where the $f_{7/2}$ orbital is located just above the neutron 82 core.

All the observed negative-parity states below 5 MeV are members of the $(\pi g_{7/2} h_{11/2})$ configuration. The experimental 3_1^- state becomes the lowest negative-parity state, whereas in theory the 2_1^- state is the lowest negative-parity state, though the energy difference between the experimental and theoretical 3^- states is small. This indicates that the strength of the octupole interaction between protons is not so large even if the interaction itself is necessary.

^{132}Sb has one valence neutron hole and one valence proton particle. So far this nucleus has been treated using only

the neutron-proton QQ interaction in the present model. Experimental energies of the 8_1^- and 9_1^- states are located at $0.0 + x$ keV and $1.025 + x$ MeV, respectively, and x is estimated as $x = 0.15\text{--}0.25$ MeV [25]. These two states are shown in Fig. 9 assuming $x = 0.20$ MeV.

Observed negative-parity states are supposed as members of the $(\nu h_{11/2}^{-1} \pi g_{7/2})$ configuration which makes $2^-, 3^-, \dots, 9^-$ states. The experimental 9_1^- state is especially higher compared to other spin states. On the other hand, the 8_1^- state, which is the neighboring spin state to the 9_1^- state, is the lowest negative-parity state among members in experiment. This feature has not been reproduced in the present interaction. As mentioned before, only the QQ interaction has been employed for the neutron-proton interaction. New kinds of interactions besides the QQ interaction should be introduced to reproduce the energy gap between the 8_1^- and 9_1^- states.

To examine the necessity of the new kind of the interactions, single- j calculations are phenomenologically performed. In this calculation, new kinds of higher-multipole interactions between the neutron $h_{11/2}$ orbital and the proton $g_{7/2}$ orbital are introduced in addition to the QQ interaction. The definition of interaction strengths are given in Appendix B. In Fig. 10 the results are shown using the hexadecapole interaction [$\chi^{(4)} = +5.00$ MeV] and the dipole interaction [$\chi^{(1)} = +1.30$ MeV] in addition to the quadrupole [$\chi^{(2)} = +8.00$ MeV] interaction between neutrons and protons in each single- j orbital (the neutron $h_{11/2}$ and proton $g_{7/2}$ orbitals). Theoretical energy of the 8^- state is adjusted to the experimental one. Using this new interaction the 8^- state becomes the lowest state and the energy gap between the 8^- and 9^- states is reproduced as seen in the figure. In Refs. [91,92], this large energy gap between the 8_1^- and the 9_1^- states was also reproduced in a SM treatment, where a two-body effective interaction derived from the Bonn A nucleon-nucleon potential was used.

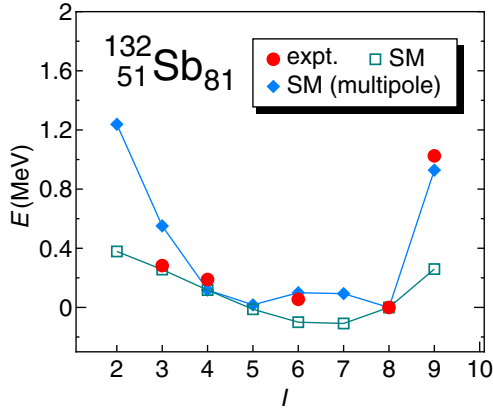


FIG. 10. (Color online) Comparison between the experimental energy levels (expt.) and two kinds of calculated results for ^{132}Sb using phenomenological neutron-proton two-body interactions: the shell-model results (SM) with only the QQ interaction and the SM results including multipole interactions [SM(multipole)].

2. ^{135}Cs

The $19/2_1^-$ state at 1.63 MeV for ^{135}Cs is a long-lived spin-gap isomer with a half-life of 53(2) min [60]. Employing the current interactions (Table II), we have failed in reproducing the situation that no $15/2^-$ and $17/2^-$ states should appear below the $19/2_1^-$, as seen in Fig. 7. Thus we need to modify the interaction in order to realize this situation.

Figure 11 shows the energy spectra for ^{135}Cs with a modified interaction. The strengths of two-body interactions are the same as in Table II, but the single-particle energy of the proton $g_{7/2}$ orbital is changed. Here $\epsilon_\pi(g_{7/2}) = -0.300$ MeV is used instead of $\epsilon_\pi(g_{7/2}) = 0.120$ MeV in Fig. 7. With this

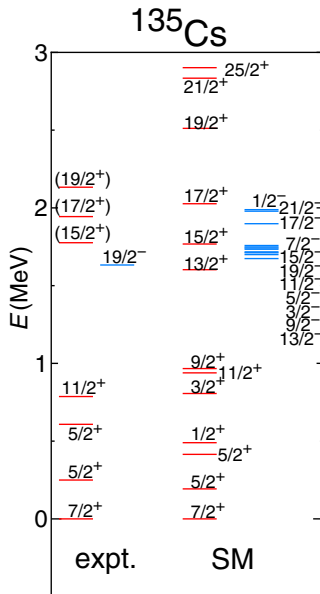


FIG. 11. (Color online) Comparison between the experimental energy levels (expt.) and the calculated results (SM) with modified interactions for ^{135}Cs . The experimental data are taken from Refs. [29,60,76].

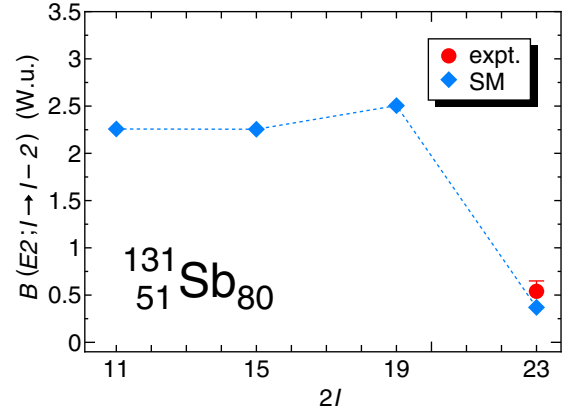


FIG. 12. (Color online) Experimental and theoretical $B(E2; I \rightarrow I - 2)$ values (in W.u.) in ^{131}Sb . The filled circles in red and diamonds in blue represent the experimental data (expt.) and the theoretical results (SM), respectively. The experimental data are taken from Ref. [39].

new interaction, we have succeeded in getting the $19/2_1^-$ state lower than the $15/2_1^-$ and $17/2_1^-$ states. Experimental study for this nucleus and its detailed theoretical analyses were carried out in Ref. [76].

3. ^{131}Sb isomers

In ^{131}Sb , the $23/2_1^+$ state at 2.17 MeV is an isomer with a half-life of 1.1(2) μs [39]. In experiment this state only decays to the $19/2_1^+$ state at 2.07 MeV by the $E2$ transition. Figure 12 shows a comparison between the experimental and theoretical $B(E2)$ values. The calculated $B(E2; 23/2_1^+ \rightarrow 19/2_1^+)$ value (0.370 W.u.) reproduces the small experimental data [0.54(11) W.u.]. This small $B(E2)$ value makes the $23/2_1^+$ state an isomer. In order to understand why this specific $B(E2)$ value becomes small, the wave function of each state is investigated. Since the $19/2_1^+$ and $23/2_1^+$ states have turned out to consist of the $(\pi g_{7/2} \nu h_{11/2}^{-2})$ configuration for more than 99%, single- j shell calculations are carried as follows.

Figure 13 shows energy vs spin diagrams with the $(\pi g_{7/2} \nu h_{11/2}^{-2})$ configuration. It should be noted that here each energy is calculated in terms of the pure $(\pi g_{7/2} \nu h_{11/2}^{-2})$ configuration without diagonalizing the Hamiltonian. Namely energy of each state with spin I is calculated as

$$E_I[\pi g_{7/2} \nu (h_{11/2}^{-2})_{J^+}] = \langle \pi g_{7/2} \nu (h_{11/2}^{-2})_{J^+}; I | \hat{H} | \pi g_{7/2} \nu (h_{11/2}^{-2})_{J^+}; I \rangle. \quad (38)$$

Here $\nu (h_{11/2}^{-2})_{J^+}$ stands for the neutron hole pair in the neutron $h_{11/2}$ orbital with spin-parity J^+ . Through the analysis of wave functions in terms of the occupation numbers, the $19/2_1^+$ state belongs to the $[\pi g_{7/2} \nu (h_{11/2}^{-2})_6^+]$ configuration. In contrast, the $23/2_1^+$ state belongs to the $[\pi g_{7/2} \nu (h_{11/2}^{-2})_{10^+}]$ configuration. In this case the $B(E2; 23/2_1^+ \rightarrow 19/2_1^+)$ value should be zero because of the spin-four change for the neutron part wave functions. In reality the $B(E2)$ value is not completely zero because of the configuration mixing by a small amount of the QQ interaction. By this admixture, the $E2$ transition rate from

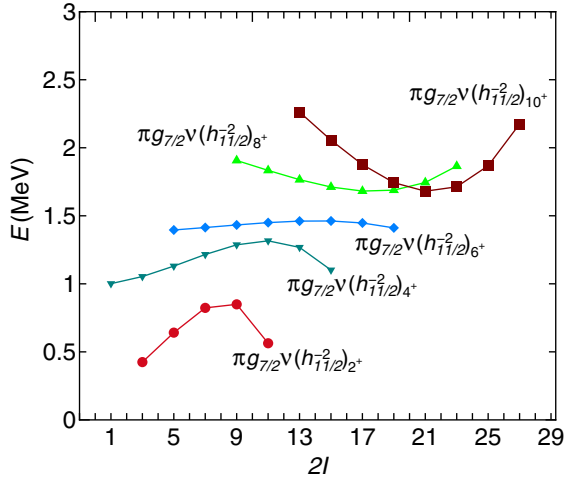


FIG. 13. (Color online) Energy (E) versus spin (I) diagram for calculated energies with assumed configurations $[\pi g_{7/2} v (h_{11/2}^{-2})_J^+]$ for ^{131}Sb .

the $23/2_2^+$ state with the $[\pi g_{7/2} v (h_{11/2}^{-2})_{8^+}]$ configuration to the $19/2_1^+$ state becomes 1.10 W.u. in the full SM calculation.

4. Seniority isomers: ^{136}Xe and Sn isotopes

Here the isomeric 6_1^+ state at 1.89 MeV with a half-life of $2.95 \mu\text{s}$ [66] in ^{136}Xe is discussed. This is a single-closed nucleus with four valence protons. Figure 14 shows theoretical $B(E2)$ values [SM(full)] in comparison with the experimental data. It is seen from the figure that the present calculations reproduce the experimental data well. The measured $B(E2; 6_1^+ \rightarrow 4_1^+)$ value is over two orders of magnitude smaller compared to other $B(E2)$ values.

In a single-closed nucleus the seniority isomer can be a candidate for an isomeric state. In a single- j shell case the $E2$ transition matrix element between two states with the same seniority v and the valence particle number n is given by

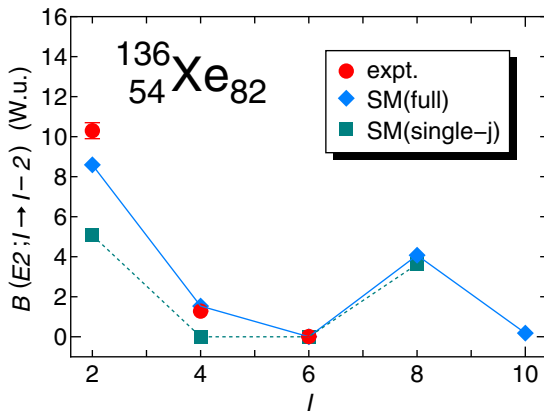


FIG. 14. (Color online) Experimental and theoretical $B(E2; I \rightarrow I - 2)$ values (in W.u.) in ^{136}Xe . The filled circles in red and diamonds in blue represent the experimental value (expt.) and the theoretical results in the full SM calculation [SM(full)], respectively. The squares in green indicate single- j results [SM(single- j)]. The experimental data are taken from Ref. [66].

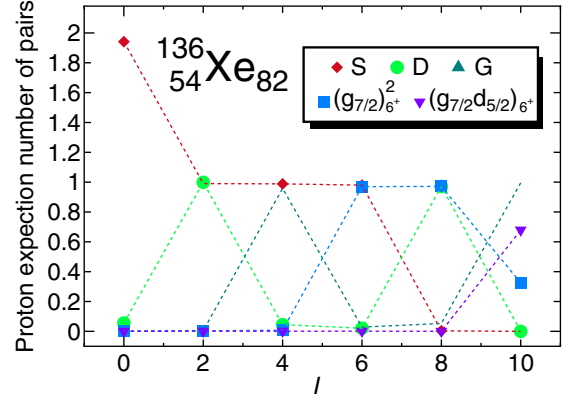


FIG. 15. (Color online) The expectation numbers of proton pairs in each state calculated by the PTSM for ^{136}Xe . S , D , G , $(g_{7/2})_{6^+}^2$ and $(g_{7/2}d_{5/2})_{6^+}$ represent the proton S pair, D pair, G pair, $(g_{7/2})_{6^+}^2$ pair, and $(g_{7/2}d_{5/2})_{6^+}$ pair, respectively.

Ref. [93],

$$\langle j^n v J_f || \hat{Q} || j^n v J_i \rangle = \frac{\Omega - n}{\Omega - v} \langle j^v v J_f || \hat{Q} || j^v v J_i \rangle, \quad (39)$$

where $\Omega = j + 1/2$ is degeneracy and \hat{Q} is any quadrupole operator. In the case with $\Omega = n$, this matrix element vanishes. This is exactly applicable in ^{136}Xe assuming $\Omega = 4$ ($j = g_{7/2}$) and $n = 4$.

Figure 15 shows expectation numbers of proton pairs for low-lying states calculated by the PTSM. The S , D , and G pairs are the same as in Refs. [12–14]. The $(g_{7/2})_{6^+}^2$ pair is a noncollective pair coupled to maximum spin ($K = 6$) in the proton $g_{7/2}$ orbital and the $(g_{7/2}d_{5/2})_{6^+}$ pair is a noncollective pair coupled to maximum spin 6 in the proton $g_{7/2}$ and $d_{5/2}$ orbitals. As seen in the figure, the ground state has seniority $v = 0$ (only made of two S pairs). The 2_1^+ , 4_1^+ , and 6_1^+ states have seniority $v = 2$ (made of one S pair and one other pair). The 4_1^+ state is mainly made of one S pair and one G pair. On the other hand, the 6_1^+ state is mainly made of one S pair and one $(g_{7/2})_{6^+}^2$ pair. The $B(E2; 4_1^+ \rightarrow 2_1^+)$ value is not small in spite of the fact that the 2_1^+ state also has $v = 2$. This is due to the contribution from other orbitals than the $g_{9/2}$ orbital. Figure 14 also shows the $B(E2)$ values calculated assuming the single- j ($g_{9/2}$) orbital alone. In the single- j shell calculation, the $B(E2; 4_1^+ \rightarrow 2_1^+)$ and $B(E2; 6_1^+ \rightarrow 4_1^+)$ values completely vanish as concluded from Eq. (39). The difference of the $B(E2; 4_1^+ \rightarrow 2_1^+)$ value between the full SM result and the single- j result comes from the contribution of orbitals other than the $g_{7/2}$ orbital; in particular, contributions of the $d_{3/2}$ and $s_{1/2}$ orbitals are large. On the contrary, there is only a small difference between the full result and the single- j result for the $B(E2; 6_1^+ \rightarrow 4_1^+)$ and $B(E2; 8_1^+ \rightarrow 6_1^+)$ values. The single- j description is sufficient to describe these transition rates. It should be noted that in a four-particle system the 10^+ state cannot be made of particles in the $g_{7/2}$ orbital alone.

Similarly, states in ^{126}Sn can become seniority isomers assuming the single- j shell with $\Omega = 6$ ($j = h_{11/2}$) and $n = 6$. As seen in Table III, theoretical $B(E2; I \rightarrow I - 2)$ values ($I = 4, 6, 8, 10$) in ^{126}Sn become quite small. It is also seen

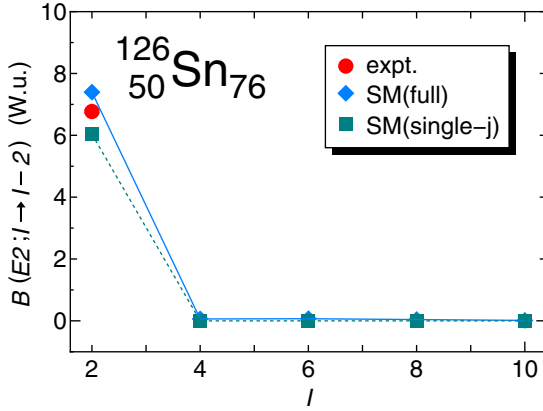


FIG. 16. (Color online) Experimental and theoretical $B(E2; I \rightarrow I - 2)$ values (in W.u.) in ^{126}Sn . The filled circles in red and diamonds in blue represent the experimental data (expt.) and the theoretical results in the full SM calculation [SM (full)], respectively. The squares in green indicate single- j results [SM (single- j)]. The experimental data are taken from Ref. [36].

that $B(E2; I \rightarrow I - 2)$ values become small as n approaches six from two (from ^{130}Sn to ^{126}Sn).

Figure 16 shows theoretical $B(E2)$ values for ^{126}Sn in comparison with the experimental data. Here SM(full) indicates the $B(E2)$ values in the full SM and the SM(single- j) indicates those in the single- j shell of the $h_{11/2}$ orbital. In the single- j shell calculation seniority $v = 2$ is assumed for the $I \geq 2$ states. It is well known that the single- j picture is valid for the low-lying yrast states in even-even Sn isotopes. The present calculation shows that the occupation probabilities of neutrons in the $h_{11/2}$ orbital for 2_1^+ states are 90%, 82%, and 80% for ^{130}Sn , ^{128}Sn , and ^{126}Sn , respectively. Those occupation probabilities for 4_1^+ , 6_1^+ , and 8_1^+ states are around 99% for ^{130}Sn , whereas they are around 85% and 82% for ^{128}Sn and ^{126}Sn , respectively. The validity of single- j approximation is also confirmed in the present model.

Table XVIII shows the calculated $B(E2)$ values for the two-valence-neutron system of ^{130}Sn in the single- j model in comparison with the full SM. The differences between the two models are less than 1.2 times. It is found that the single- j shell picture well describes the full SM results with respect to the $B(E2)$ values.

IV. SUMMARY

In this paper the energy spectra and electromagnetic transitions in even-even, odd-mass, and doubly-odd nuclei with mass around 130 are investigated by a shell-model approach.

TABLE XVIII. Calculated $B(E2; I \rightarrow I - 2)$ values (in W.u.) in a two-particle system (^{130}Sn) assuming a single- j shell (single- j) in comparison with the full SM results (full).

I	2^+	4^+	6^+	8^+	10^+
Full	1.52	1.45	1.43	0.871	0.330
Single- j	1.41	1.74	1.42	0.880	0.330

The effective interactions consist of single-particle energies and phenomenological two-body effective interactions, which mainly consist of the monopole and quadrupole pairing plus quadrupole-quadrupole interaction. In order to more accurately reproduce the spectra in odd-mass nuclei, we have assumed that single-particle energies of the neutron $0h_{11/2}$ orbital and the proton $0g_{7/2}$ orbital changes linearly with the numbers of valence neutron holes and proton particles. We employ only one set of two-body interactions, whose strengths are fixed constant for all the nuclei.

In this shell-model framework, we have taken the method of diagonalizing the neutron system and the proton system, separately, and, finally, the neutron-proton system. This method has turned out to be efficient and useful, indicating that in this mass region of a few valence nucleons between 50 and 82, interactions between alike nucleons are not so strong compared to those interactions between like nucleons.

Energy spectra are calculated for Sn, Sb, Te, I, Xe, Cs, and Ba isotopes around mass 130. We have obtained good agreements with the experimental observations in most of the nuclei. However, we have found large discrepancies between experiment and theory in some cases. In particular, large differences in energy levels are seen in many valence-nucleon systems, partly because we have fixed two-body interactions in a few valence-nucleon systems. Furthermore, large differences are also seen in doubly-odd nuclei.

For a better description of each nucleus, we need to treat each nucleus separately with modified strengths of interactions or by introducing other kinds of interactions which are not considered in the present model. Intensive studies have been made in some cases by modifying the effective interactions. For example, we have found in ^{132}Sb that we need other types of interactions between neutrons and protons besides the $Q_\nu Q_\pi$ interaction. Moreover, from the fact that negative-parity states are not reproduced well in some odd-mass nuclei, effective interactions for negative-parity states might be required, such as an interaction between the neutron $h_{11/2}$ orbital and the proton $g_{7/2}$ orbital.

In this calculation, two-body interactions which directly affect the negative-parity states have not been introduced. Instead, the effect of such interactions for the negative-parity states has been compensated by changing the single-particle energy of the neutron $h_{11/2}$ orbital as a function of valence neutron and proton numbers. The introduction of such new kinds of two-body interactions will be one of our future projects.

With respect to octupole interactions, which are known to be important in superheavy nuclei, such as Ra, Th, and U isotopes, we find only a small necessity of introducing them among like nucleons in this mass region. In fact, in even-even Sn isotopes (single-closed nuclei), the spin-parity of the lowest negative-parity state is not 3^- . In ^{126}Sn we have reproduced the first 3^- state almost at the right position without introducing any octupole interactions. In contrast, the spin-parity of the lowest negative-parity state is 3^- for neutron magic single-closed nuclei ($N = 82$). Thus we might need octupole interactions between protons for a better description, but importance of the interaction is not so large.

Through this work, although it has not been mentioned in the main text, it is also found necessary to introduce

the interaction between the neutron in the $h_{11/2}$ orbital and the proton in the $h_{11/2}$ orbital in order to describe almost degenerate $\Delta I = 1$ doublet bands with the same parity, which systematically appear in this mass region.

Electromagnetic transition rates and moments are also calculated and well reproduced as a whole. We have assumed a number dependence on the effective charges. In the light mass region, the effects and importance of the tensor force and/or the monopole interactions on the single-particle energies and transition rates were discussed in Refs. [94,95]. The number dependence on the single-particle energies and the effective charges, which are introduced phenomenologically in the present work, might be compensated by introduction of these interactions. It should be noted, however, that in the present treatment the number dependence on the effective charges is not so large, and transition rates are not much changed even without the particle number dependence of the effective charge in the present calculation.

As for magnetic moments and quadrupole moments, generally speaking, the magnetic dipole moments agree with the experimental data much better than the electric quadrupole moments.

Some isomeric states are analyzed using the pair-truncated shell model as well as the shell model. It turns out that some isomers in this mass region originate from the large structural change of wave functions, although most of the isomers are concluded as spin-gap isomers.

ACKNOWLEDGMENTS

The numerical calculations financially supported by Saitama University were carried out partly by the HITACHI SR16000 supercomputers at Supercomputing Division, Information Technology Center, University of Tokyo. This work was supported by Grant-in-Aid for Scientific Research (C) (Grants No. 24540251 and No. 25400267) from Japan Society for the Promotion of Science (JSPS) and also by a Grant-in-Aid for JSPS Fellows (Grant No. 26.10429).

APPENDIX A: MATRIX ELEMENTS OF TWO-BODY INTERACTIONS BETWEEN LIKE NUCLEONS

In this appendix we explicitly give the two-body matrix elements $\langle i_1 i_2; J | \hat{H} | i_3 i_4; J \rangle$ for two-body interactions between like nucleons in terms of their interaction strengths. Here in generic i_k , ($k = 1, 2, 3, 4$) represents isotropic harmonic oscillator quantum numbers (n, ℓ, j) with spin degrees of freedom. The matrix element $\langle i_1 i_2; J | \hat{H} | i_3 i_4; J \rangle$ is evaluated between the normalized, but not antisymmetrized wave functions $|i_1 i_2; J\rangle$ and $|i_3 i_4; J\rangle$. The antisymmetrized matrix element should be calculated as

$$\begin{aligned} & \langle i_1 i_2; J | \hat{H} | i_3 i_4; J \rangle_A \\ &= \frac{1}{4} [\langle i_1 i_2; J | \hat{H} | i_3 i_4; J \rangle \\ & - (-1)^{i_1+i_2-J} \langle i_2 i_1; J | \hat{H} | i_3 i_4; J \rangle \\ & - (-1)^{i_3+i_4-J} \langle i_1 i_2; J | \hat{H} | i_4 i_3; J \rangle \\ & + (-1)^{i_1+i_2+i_3+i_4} \langle i_2 i_1; J | \hat{H} | i_4 i_3; J \rangle]. \end{aligned} \quad (\text{A1})$$

In the following, two-body matrix elements are given term by term.

The monopole pairing interaction, $\hat{H} = -G_0 \hat{P}^{\dagger(0)} \hat{P}^{(0)}$, becomes

$$\begin{aligned} & \langle i_1 i_2; J | \hat{H} | i_3 i_4; J \rangle \\ &= -G_0 \delta_{j_0} \sqrt{(j_1 + \frac{1}{2})(j_3 + \frac{1}{2})} \delta_{i_1 i_2} \delta_{i_3 i_4}. \end{aligned} \quad (\text{A2})$$

The quadrupole-pairing interaction, $\hat{H} = -G_2 \hat{P}^{\dagger(2)} \cdot \hat{P}^{(2)}$, becomes

$$\begin{aligned} & \langle i_1 i_2; J | \hat{H} | i_3 i_4; J \rangle \\ &= -4G_2 \delta_{J2} \frac{1}{\sqrt{(1 + \delta_{i_1 i_2})(1 + \delta_{i_3 i_4})}} Q_{i_1 i_2}^{(2)} \cdot Q_{i_3 i_4}^{(2)}. \end{aligned} \quad (\text{A3})$$

Here the matrix element $Q_{i_1 i_2}^{(2)}$ is given by

$$Q_{i_1 i_2}^{(2)} = \langle n_1 \ell_1 | r^2 | n_2 \ell_2 \rangle T, \quad (\text{A4})$$

with

$$T = -\sqrt{\frac{2j_2 + 1}{4\pi}} \left(j_2 \frac{1}{2} 20 \left| j_1 \frac{1}{2} \right. \right) (-1)^{j_2 - j_1} \frac{(-1)^{\ell_1 + \ell_2} + 1}{2}. \quad (\text{A5})$$

Here the phase convention $(-1)^{n_1+n_2}$ is adopted for the calculation of $\langle n_1 \ell_1 | r^2 | n_2 \ell_2 \rangle$.

The quadrupole-quadrupole interaction, $\hat{H} = -\kappa \hat{Q} \cdot \hat{Q}$, becomes

$$\begin{aligned} & \langle i_1 i_2; J | \hat{H} | i_3 i_4; J \rangle \\ &= \frac{-20\kappa (-1)^{j_2+j_3}}{\sqrt{(1 + \delta_{i_1 i_2})(1 + \delta_{i_3 i_4})}} \left\{ \begin{matrix} j_1 & j_4 & 2 \\ j_3 & j_2 & J \end{matrix} \right\} Q_{i_1 i_2}^{(2)} \cdot Q_{i_3 i_4}^{(2)}, \end{aligned} \quad (\text{A6})$$

where $\left\{ \begin{matrix} j_1 & j_4 & 2 \\ j_3 & j_2 & J \end{matrix} \right\}$ represents a six- j coefficient.

The multipole-pairing interaction, $\hat{H} = -G_K \hat{P}^{\dagger(K)} \cdot \hat{P}^{(K)}$ ($K = 4, 6, 8, 10$), becomes

$$\begin{aligned} & \langle i_1 i_2; J | \hat{H} | i_3 i_4; J \rangle \\ &= -4G_K \delta_{JK} \frac{1}{\sqrt{(1 + \delta_{i_1 i_2})(1 + \delta_{i_3 i_4})}} Q_{i_1 i_2}^{(K)} \cdot Q_{i_3 i_4}^{(K)}. \end{aligned} \quad (\text{A7})$$

The matrix element $Q_{i_1 i_2}^{(K)}$ ($K = 4, 6, 8, 10$) is given by

$$\begin{aligned} Q_{i_1 i_2}^{(K)} &= -\sqrt{\frac{2j_2 + 1}{4\pi}} (-1)^{n_1+n_2+j_2-j_1} \left(j_2 \frac{1}{2} K 0 \left| j_1 \frac{1}{2} \right. \right) \\ &\quad \times \frac{(-1)^{\ell_1 + \ell_2} + 1}{2}. \end{aligned} \quad (\text{A8})$$

Here $\langle n_1 \ell_1 | r^K | n_2 \ell_2 \rangle = (-1)^{n_1+n_2}$ is employed. Namely, no radial dependence is considered except for the phase dependence.

APPENDIX B: NEUTRON-PROTON INTERACTIONS FOR SINGLE- j SHELLS

We define the effective interactions between one neutron in the single j_ν shell and one proton in the single j_π shell. They are given as

$$\hat{H}_{\nu\pi} = \sum_{J=0}^{J_{\max}} \chi^{(J)} \hat{U}^{(J)}(j_\nu) \cdot \hat{U}^{(J)}(j_\pi), \quad (\text{B1})$$

where J_{\max} is the highest spin and the $\chi^{(J)}$'s are parameters to be determined. The multipole particle-hole operator $\hat{U}_M^{(J)}(j)$

with the total spin J and its projection M is defined as

$$\begin{aligned} \hat{U}_M^{(J)}(j) &= \frac{1}{\sqrt{2J+1}} \sum_{m_1 m_2} (j m_1 j m_2 | J M) c_{j m_1}^\dagger \tilde{c}_{j m_2} \\ &= \frac{1}{\sqrt{2J+1}} [c_j^\dagger \tilde{c}_j]_M^{(J)}. \end{aligned} \quad (\text{B2})$$

The two-body matrix element for the state $|j_\nu j_\pi; L\rangle$ is given as

$$\begin{aligned} \langle j_\nu j_\pi; L | \hat{H}_{\nu\pi} | j_\nu j_\pi; L \rangle \\ = (-1)^{L+j_\nu+j_\pi} \sum_{J=0}^{J_{\max}} \chi^{(J)} \begin{Bmatrix} j_\nu & j_\pi & L \\ j_\pi & j_\nu & J \end{Bmatrix}. \end{aligned} \quad (\text{B3})$$

-
- [1] G. H. Lang, C. W. Johnson, S. E. Koonin, and W. E. Ormand, *Phys. Rev. C* **48**, 1518 (1993).
- [2] M. Honma, T. Mizusaki, and T. Otsuka, *Phys. Rev. Lett* **75**, 1284 (1995).
- [3] N. Yoshinaga and A. Arima, *Phys. Rev. C* **81**, 044316 (2010).
- [4] N. Shimizu, Y. Utsuno, T. Mizusaki, M. Honma, Y. Tsunoda, and T. Otsuka, *Phys. Rev. C* **85**, 054301 (2012).
- [5] T. Koike, K. Starosta, C. J. Chiara, D. B. Fossan, and D. R. LaFosse, *Phys. Rev. C* **63**, 061304(R) (2001).
- [6] I. Kuti, J. Timár, D. Sohler, E. S. Paul, K. Starosta, A. Astier, D. Bazzacco, P. Bednarczyk, A. J. Boston, N. Buforn, H. J. Chantler, C. J. Chiara, R. M. Clark, M. Cromaz, M. Descovich, Z. Dombrádi, P. Fallon, D. B. Fossan, C. Fox, A. Gizon, J. Gizon, A. A. Hecht, N. Kintz, T. Koike, I. Y. Lee, S. Lunardi, A. O. Macchiavelli, P. J. Nolan, B. M. Nyakó, C. M. Petrache, J. A. Sampson, H. C. Scraggs, T. G. Tornyi, R. Wadsworth, A. Walker, and L. Zolnai, *Phys. Rev. C* **87**, 044323 (2013).
- [7] D. J. Hartley, L. L. Riedinger, M. A. Riley, D. L. Balabanski, F. G. Kondev, R. W. Laird, J. Pfohl, D. E. Archer, T. B. Brown, R. M. Clark, M. Devlin, P. Fallon, I. M. Hibbert, D. T. Joss, D. R. LaFosse, P. J. Nolan, N. J. O'Brien, E. S. Paul, D. G. Sarantites, R. K. Sheline, S. L. Shepherd, J. Simpson, R. Wadsworth, J. Y. Zhang, P. B. Semmes, and F. Döna, *Phys. Rev. C* **64**, 031304(R) (2001).
- [8] A. Johnson, H. Ryde, and S. A. Hjorth, *Nucl. Phys. A* **179**, 753 (1972).
- [9] J. J. Valiente-Dobon, P. H. Regan, C. Wheldon, C. Y. Wu, N. Yoshinaga, K. Higashiyama, J. F. Smith, D. Cline, R. S. Chakravarthy, R. Chapman, M. Cromaz, P. Fallon, S. J. Freeman, A. Gorgen, W. Gelletly, A. Hayes, H. Hua, S. D. Langdown, I. Y. Lee, X. Liang, A. O. Macchiavelli, C. J. Pearson, Z. Podolyak, G. Sletten, R. Teng, D. Ward, D. D. Warner, and A. D. Yamamoto, *Phys. Rev. C* **69**, 024316 (2004).
- [10] R. Leguillon, H. Nishibata, Y. Ito, C. M. Petrache, A. Odahara, T. Shimoda, N. Hamatani, K. Tajiri, J. Takatsu, R. Yokoyama, E. Ideguchi, H. Watanabe, Y. Wakabayashi, K. Yoshinaga, T. Suzuki, S. Nishimura, D. Beaume, G. Lehaut, D. Guinet, P. Desesquelles, D. Curien, A. Astier, T. Konstantinopoulos, and T. Zerouki, *Phys. Rev. C* **88**, 044309 (2013).
- [11] H. Nishibata, R. Leguillon, A. Odahara, T. Shimoda, C. M. Petrache, Y. Ito, J. Takatsu, K. Tajiri, N. Hamatani, R. Yokoyama, E. Ideguchi, H. Watanabe, Y. Wakabayashi, K. Yoshinaga, T. Suzuki, S. Nishimura, D. Beaume, G. Lehaut, D. Guinet, P. Desesquelles, D. Curien, K. Higashiyama, and N. Yoshinaga, *Phys. Rev. C* **91**, 054305 (2015).
- [12] N. Yoshinaga and K. Higashiyama, *Phys. Rev. C* **69**, 054309 (2004).
- [13] K. Higashiyama and N. Yoshinaga, *Phys. Rev. C* **83**, 034321 (2011).
- [14] K. Higashiyama and N. Yoshinaga, *Phys. Rev. C* **88**, 034315 (2013).
- [15] L. Y. Jia, H. Zhang, and Y. M. Zhao, *Phys. Rev. C* **75**, 034307 (2007).
- [16] L. Y. Jia, H. Zhang, and Y. M. Zhao, *Phys. Rev. C* **76**, 054305 (2007).
- [17] K. Higashiyama and N. Yoshinaga, *Prog. Theor. Phys.* **113**, 1139 (2005).
- [18] K. Higashiyama, N. Yoshinaga, and K. Tanabe, *Phys. Rev. C* **72**, 024315 (2005).
- [19] N. Yoshinaga and K. Higashiyama, *J. Phys. G* **31**, S1455 (2005).
- [20] K. Higashiyama and N. Yoshinaga, *Eur. Phys. J. A* **33**, 355 (2007).
- [21] K. Higashiyama, N. Yoshinaga, and K. Tanabe, *Phys. Rev. C* **65**, 054317 (2002).
- [22] A. hashizume, *Nucl. Data Sheets.* **112**, 1647 (2011).
- [23] M. kanbe and K. kitao, *Nucl. Data Sheets.* **94**, 227 (2001).
- [24] Y. Tendow, *Nucl. Data Sheets.* **77**, 631 (1996).
- [25] B. Singh, *Nucl. Data Sheets.* **93**, 33 (2001).
- [26] A. Astier, M.-G. Porquet, C. Theisen, D. Verney, I. Deloncle, M. Houry, R. Lucas, F. Azaiez, G. Barreau, D. Curien, O. Dorvaux, G. Duchêne, B. J. P. Gall, N. Redon, M. Rousseau, and O. Stézowski, *Phys. Rev. C* **85**, 054316 (2012).
- [27] S. Pietri, A. Jungclaus, M. Górski, H. Grawe, M. Pfützner, L. Cáceres, P. Detistov, S. Lalkowski, V. Modamio, Z. Podolyak, P. H. Regan, D. Rudolph, J. Walker, E. Werner-Malento, P. Bednarczyk, P. Doornenbal, H. Geissel, J. Gerl, J. Grebosz, I. Kojouharov, N. Kurz, W. Prokopowicz, H. Schaffner, H. J. Wollersheim, K. Andgren, J. Benlliure, G. Benzoni, A. M. Bruce, E. Casarejos, B. Cederwall, F. C. L. Crespi, B. Hadinia, M. Hellström, R. Hoischen, G. Ilie, A. Khaplanov, M. Kmiecik, R. Kumar, A. Maj, S. Mandal, F. Montes, S. Myalski, G. Simpson, S. J. Steer, S. Tashenov, and O. Wieland, *Phys. Rev. C* **83**, 044328 (2011).
- [28] L. W. Iskra, R. Broda, R. V. F. Janssens, J. Wrzesiński, B. Szpak, C. J. Chiara, M. P. Carpenter, B. Fornal, N. Hoteling, F. G.

- Kondev, W. Królas, T. Lauritsen, T. Pawlat, D. Seweryniak, I. Stefanescu, W. B. Walters, and S. Zhu, *Phys. Rev. C* **89**, 044324 (2014).
- [29] *Evaluated Nuclear Structure Data File* (ENSDF), [<http://www.nndc.bnl.gov/ensdf/>].
- [30] G. J. Kumbartzki, N. Benczer-Koller, D. A. Torres, B. Manning, P. D. O'Malley, Y. Y. Sharon, L. Zamick, C. J. Gross, D. C. Radford, S. J. Q. Robinson, J. M. Allmond, A. E. Stuchbery, K.-H. Speidel, N. J. Stone, and C. R. Bingham, *Phys. Rev. C* **86**, 034319 (2012).
- [31] C. T. Zhang, P. Bhattacharyya, P. J. Daly, Z. W. Grabowski, R. Broda, B. Fornal, and J. Blomqvist, *Phys. Rev. C* **62**, 057305 (2000).
- [32] J. M. Allmond, D. C. Radford, C. Baktash, J. C. Batchelder, A. Galindo-Uribarri, C. J. Gross, P. A. Hausladen, K. Lagergren, Y. Larochele, E. Padilla-Rodal, and C.-H. Yu, *Phys. Rev. C* **84**, 061303(R) (2011).
- [33] J. M. Allmond, A. E. Stuchbery, D. C. Radford, A. Galindo-Uribarri, N. J. Stone, C. Baktash, J. C. Batchelder, C. R. Bingham, M. Danchev, C. J. Gross, P. A. Hausladen, K. Lagergren, Y. Larochele, E. Padilla-Rodal, and C.-H. Yu, *Phys. Rev. C* **87**, 054325 (2013).
- [34] N. Stone, *Atomic Data and Nuclear Data Tables*. **90**, 75 (2005).
- [35] N. Stone, *Table of Nuclear Magnetic Dipole and Electric Quadrupole Moments* (International Nuclear Data Committee, Oxford, 2014).
- [36] J. Katakura and K. Kitao, *Nucl. Data Sheets*. **97**, 765 (2002).
- [37] R. L. Lozeva, G. S. Simpson, H. Grawe, G. Neyens, L. A. Atanasova, D. L. Balabanski, D. Bazzacco, F. Becker, P. Bednarczyk, G. Benzoni, N. Blasi, A. Blazhev, A. Bracco, C. Brandau, L. Cáceres, F. Camera, S. K. Chamoli, F. C. L. Crespi, J.-M. Daugas, P. Detistov, M. D. Rydt, P. Doornenbal, C. Fahlander, E. Farnea, G. Georgiev, J. Gerl, K. A. Gladnishki, M. Górska, J. Grebosz, M. Hass, R. Hoischen, G. Ilie, M. Ionescu-Bujor, A. Iordachescu, J. Jolie, A. Jungclaus, M. Kmiecik, I. Kojouharov, N. Kurz, S. P. Lakshmi, G. L. Bianco, S. Mallion, A. Maj, D. Montanari, O. Perru, M. Pfützner, S. Pietri, J. A. Pinston, Z. Podolyák, W. Prokopowicz, D. Rudolph, G. Rusev, T. R. Saitoh, A. Saltarelli, H. Schaffner, R. Schwengner, S. Tashenov, K. Turzó, J. J. Valiente-Dobón, N. Vermeulen, J. Walker, E. Werner-Malento, O. Wieland, and H.-J. Wollersheim, *Phys. Rev. C* **77**, 064313 (2008).
- [38] M. Lindroos, M. Booth, D. Doran, Y. Koh, I. Oliveira, J. Rikowska, P. Richards, N. J. Stone, M. Veskovc, D. Zákoucky, and B. Fogelberg, *Phys. Rev. C* **53**, 124 (1996).
- [39] Y. Khazov, I. Mitropolsky, and A. Rodionov, *Nucl. Data Sheets*. **107**, 2715 (2006).
- [40] Y. Khazov, A. A. Rodionov, S. Sakharov, and B. Singh, *Nucl. Data Sheets*. **104**, 497 (2005).
- [41] J. Genevey, J. A. Pinston, C. Foin, M. Rejmund, H. Faust, and B. Weiss, *Phys. Rev. C* **65**, 034322 (2002).
- [42] H. Watanabe, G. J. Lane, G. D. Dracoulis, A. P. Byrne, P. Nieminen, F. G. Kondev, K. Ogawa, M. P. Carpenter, R. V. F. Janssens, T. Lauritsen, D. Seweryniak, S. Zhu, and P. Chowdhury, *Eur. Phys. J. A* **42**, 163 (2009).
- [43] P. Walker and G. Dracoulis, *Nature* **399**, 35 (1999).
- [44] J. Sau and K. Heyde, *Phys. Rev. C* **23**, 2315 (1981).
- [45] J. Genevey, J. A. Pinston, H. R. Faust, R. Orlandi, A. Scherillo, G. S. Simpson, I. S. Tsekhanovich, A. Covello, A. Gargano, and W. Urban, *Phys. Rev. C* **67**, 054312 (2003).
- [46] F. Andreozzi, L. Coraggio, A. Covello, A. Gargano, T. T. S. Kuo, and A. Porrino, *Phys. Rev. C* **59**, 746 (1999).
- [47] M.-G. Porquet, T. Venkova, R. Lucas, A. Astier, A. Bauchet, I. Deloncle, A. Prévost, F. Azaiez, G. Barreau, A. Bogachev, N. Bufo, A. Buta, D. Curien, T. P. Doan, L. Donadille, O. Dorvaux, G. Duchêne, J. Durell, T. Ethvignot, B. P. J. Gall, D. Grimwood, M. Houry, F. Khalfallah, W. Korten, S. Lalkovski, Y. L. Coz, M. Meyer, A. Minkova, I. Piqueras, N. Redon, A. Roach, M. Rousseau, N. Schulz, A. G. Smith, O. Stézowski, C. Theisen, and B. J. Varley, *Eur. Phys. J. A* **24**, 39 (2005).
- [48] Y. Khazov, A. Rodionov, and F. G. Kondev, *Nucl. Data Sheets*. **112**, 855 (2011).
- [49] A. Sonzogni, *Nucl. Data Sheets*. **103**, 1 (2004).
- [50] S. F. Hicks, J. C. Boehringer, N. Boukharouba, C. Fransen, S. R. Leshner, J. M. Mueller, J. R. Vanhoy, and S. W. Yates, *Phys. Rev. C* **86**, 054308 (2012).
- [51] R. Broda, B. Fornal, W. Królas, T. Pawlat, J. Wrzesiński, D. Bazzacco, G. de Angelis, S. Lunardi, and C. R. Alvarez, *Eur. Phys. J. A* **20**, 145 (2004).
- [52] A. Astier, M.-G. Porquet, T. Venkova, C. Theisen, G. Duchêne, F. Azaiez, G. Barreau, D. Curien, I. Deloncle, O. Dorvaux, B. Gall, M. Houry, R. Lucas, N. Redon, M. Rousseau, and O. Stézowski, *Eur. Phys. J. A* **50**, 2 (2014).
- [53] J. M. Allmond, D. C. Radford, J. Pavan, K. Lagergren, C. Baktash, J. R. Beene, C. R. Bingham, L. Chaturvedi, M. Danchev, D. Fong, A. Galindo-Uribarri, P. A. Hausladen, J. K. Hwang, W. Krolas, J. F. Liang, E. Padilla-Rodal, W. Reviol, D. G. Sarantites, D. Seweryniak, D. Shapira, A. E. Stuchbery, J. P. Urrego-Blanco, R. L. Varner, X. Wang, C.-H. Yu, and S. Zhu, *Phys. Rev. C* **86**, 031307(R) (2012).
- [54] S. Abu-Musleh, H. M. Abu-Zeidb, and O. Scholten, *Nucl. Phys. A* **927**, 91 (2014).
- [55] D. C. Radford, C. Baktash, J. R. Beene, B. Fuentes, A. Galindo-Uribarri, C. J. Gross, P. A. Hausladen, T. A. Lewis, P. E. Mueller, E. Padilla, D. Shapira, D. W. Stracener, C.-H. Yu, C. J. Barton, M. A. Caprio, L. Coraggio, A. Covello, A. Gargano, D. J. Hartley, and N. V. Zamfir, *Phys. Rev. Lett.* **88**, 222501 (2002).
- [56] J. Genevey, J. A. Pinston, C. Foin, M. Rejmund, R. F. Casten, H. Faust, and S. Oberstedt, *Phys. Rev. C* **63**, 054315 (2001).
- [57] C. J. Barton, M. A. Caprio, D. Shapira, N. V. Zamfir, D. S. Brenner, R. L. Gill, T. A. Lewis, J. R. Cooper, R. F. Casten, C. W. Beausang, R. Kruckenb, and J. R. Novak, *Phys. Lett. B* **551**, 269 (2003).
- [58] N. Benczer-Koller, G. J. Kumbartzki, G. Gürdal, C. J. Gross, A. E. Stuchbery, B. Krieger, R. Hatarik, P. O'Malley, S. Pain, L. Segen, C. Baktash, J. Beene, D. C. Radford, C. H. Yu, N. J. Stone, J. R. Stone, C. R. Bingham, M. Danchev, R. Grzywacz, and C. Mazzocchi, *Phys. Lett. B* **664**, 241 (2008).
- [59] M. Danchev, G. Rainovski, N. Pietralla, A. Gargano, A. Covello, C. Baktash, J. R. Beene, C. R. Bingham, A. Galindo-Uribarri, K. A. Gladnishki, C. J. Gross, V. Y. Ponomarev, D. C. Radford, L. L. Riedinger, M. Scheck, A. E. Stuchbery, J. Wambach, C.-H. Yu, and N. V. Zamfir, *Phys. Rev. C* **84**, 061306(R) (2011).
- [60] B. Singh, A. A. Rodionov, and Y. L. Khazov, *Nucl. Data Sheets*. **109**, 517 (2008).
- [61] D. Deleanu, D. L. Balabanski, T. Venkova, D. Bucurescu, N. Marginean, E. Ganioglu, G. Cata-Danil, L. Atanasova, I. Cata-Danil, P. Detistov, D. Filipescu, D. Ghita, T. Glodariu, M. Ivascu, R. Marginean, C. Mihai, A. Negret, S. Pascu, T. Sava, L. Stroe, G. Suliman, and N. V. Zamfir, *Phys. Rev. C* **87**, 014329 (2013).

- [62] H. Jin, M. Hasegawa, S. Tazaki, K. Kaneko, and Y. Sun, *Phys. Rev. C* **84**, 044324 (2011).
- [63] S. H. Liu, J. H. Hamilton, A. V. Ramayya, J. K. Hwang, A. V. Daniel, G. M. Ter-Akopian, Y. X. Luo, J. O. Rasmussen, S. J. Zhu, and W. C. Ma, *Phys. Rev. C* **79**, 067303 (2009).
- [64] L. Coraggio, A. Covello, A. Gargano, and N. Itaco, *Phys. Rev. C* **80**, 061303(R) (2009).
- [65] H. Watanabe, G. J. Lane, G. D. Dracoulis, A. P. Byrne, P. Nieminen, F. G. Kondev, K. Ogawa, M. P. Carpenter, R. V. F. Janssens, T. Lauritsen, D. Seweryniak, S. Zhu, and P. Chowdhury, *Phys. Rev. C* **79**, 064311 (2009).
- [66] A. Sonzogni, *Nucl. Data Sheets* **95**, 837 (2002).
- [67] G. Jakob, N. Benczer-Koller, G. Kumbartzki, J. Holden, T. J. Mertzimekis, K.-H. Speidel, R. Ernst, A. E. Stuchbery, A. Pakou, P. Maier-Komor, A. Macchiavelli, M. McMahan, L. Phair, and I. Y. Lee, *Phys. Rev. C* **65**, 024316 (2002).
- [68] G. Puddu, O. Scholten, and T. Otsuka, *Nucl. Phys. A* **348**, 109 (1980).
- [69] R. F. Casten and P. von Brentano, *Phys. Lett. B* **152**, 22 (1985).
- [70] F. Iachello and A. Arima, *The Interacting Boson Model* (Cambridge University, Cambridge, 1987).
- [71] A. Sevrin, K. Heyde, and J. Jolie, *Phys. Rev. C* **36**, 2631 (1987).
- [72] T. Mizusaki and T. Otsuka, *Prog. Theor. Phys. Suppl.* **125**, 97 (1996).
- [73] O. Vogel, P. VanIsacker, A. Gelberg, P. von Brentano, and A. Dewald, *Phys. Rev. C* **53**, 1660 (1996).
- [74] A. Shrivastava, M. Caamano, M. Rejmund, A. Navin, F. Rejmund, K.-H. Schmidt, A. Lemasson, C. Schmitt, L. Gauderfroy, K. Sieja, L. Audouin, C. O. Bacri, G. Barreau, J. Benlliure, E. Casarejos, X. Derkx, B. Fernández-Dominguez, C. Golabek, B. Jurado, T. Roger, and J. Taieb, *Phys. Rev. C* **80**, 051305(R) (2009).
- [75] N. Fotiades, R. O. Nelson, M. Devlin, J. A. Cizewski, J. A. Becker, W. Younes, R. Krücken, R. M. Clark, P. Fallon, I. Y. Lee, A. O. Macchiavelli, T. Ethvignot, and T. Granier, *Phys. Rev. C* **75**, 054322 (2007).
- [76] N. Fotiades, J. A. Cizewski, K. Higashiyama, N. Yoshinaga, E. Teruya, R. Krücken, R. M. Clark, P. Fallon, I. Y. Lee, A. O. Macchiavelli, and W. Younes, *Phys. Rev. C* **88**, 064315 (2013).
- [77] E. Browne and J. K. Tuli, *Nucl. Data Sheets* **108**, 2173 (2007).
- [78] H. Pai, G. Mukherjee, A. Raghav, R. Palit, C. Bhattacharya, S. Chanda, T. Bhattacharjee, S. Bhattacharyya, S. K. Basu, A. Goswami, P. K. Joshi, B. S. Naidu, S. K. Sharma, A. Y. Deo, Z. Naik, R. K. Bhowmik, S. Muralithar, R. P. Singh, S. Kumar, S. Sihotra, and D. Mehta, *Phys. Rev. C* **84**, 041301(R) (2011).
- [79] A. Astier, M.-G. Porquet, G. Duchêne, F. Azaiez, D. Curien, I. Deloncle, O. Dorvaux, B. J. P. Gall, M. Houry, R. Lucas, P. C. Srivastava, N. Redon, M. Rousseau, O. Stézowski, and C. Theisen, *Phys. Rev. C* **87**, 054316 (2013).
- [80] A. Sonzogni, *Nucl. Data Sheets* **98**, 515 (2003).
- [81] S. Kumar, A. K. Jain, A. Goel, S. S. Malik, R. Palit, H. C. Jain, I. Mazumdar, P. K. Joshi, Z. Naik, A. Dhal, T. Trivedi, I. Mehrotra, S. Appannababu, L. Chaturvedi, V. Kumar, R. Kumar, D. Negi, R. P. Singh, S. Muralithar, R. K. Bhowmik, and S. C. Pancholi, *Phys. Rev. C* **81**, 067304 (2010).
- [82] T. Shizuma, Z. Gan, K. Ogawa, H. Nakada, M. Oshima, Y. Toh, T. Hayakawa, Y. Hatsukawa, M. Sugawara, Y. Utsuno, and Z. Liu, *Eur. Phys. J. A* **20**, 207 (2004).
- [83] A. Astier, M.-G. Porquet, T. Venkova, D. Verney, C. Theisen, G. Duchêne, F. Azaiez, G. Barreau, D. Curien, I. Deloncle, O. Dorvaux, B. J. P. Gall, M. Houry, R. Lucas, N. Redon, M. Rousseau, and O. Stézowski, *Phys. Rev. C* **85**, 064316 (2012).
- [84] L. Coquard, N. Pietralla, G. Rainovski, T. Ahn, L. Bettermann, M. P. Carpenter, R. V. F. Janssens, J. Leske, C. J. Lister, O. Möller, W. Rother, V. Werner, and S. Zhu, *Phys. Rev. C* **82**, 024317 (2010).
- [85] T. Ahn, L. Coquard, N. Pietralla, G. Rainovsk, A. Costin, R. V. F. Janssens, and C. J. Lister, *Phys. Lett. B* **679**, 19 (2009).
- [86] D. Bianco, N. Loludice, F. Andreozzi, A. Porrino, and F. Knapp, *Phys. Rev. C* **86**, 044325 (2012).
- [87] D. Bianco, F. Andreozzi, N. Loludice, A. Porrino, and F. Knapp, *Phys. Rev. C* **84**, 024310 (2011).
- [88] K. Sieja, G. Martínez-Pinedo, L. Coquard, and N. Pietralla, *Phys. Rev. C* **80**, 054311 (2009).
- [89] D. Bianco, N. Loludice, F. Andreozzi, A. Porrino, and F. Knapp, *Phys. Rev. C* **88**, 024303 (2013).
- [90] S. K. Saha, C. Constantinescu, P. J. Daly, P. Bhattacharyya, C. T. Zhang, Z. W. Grabowski, B. Fornal, R. Broda, I. Ahmad, D. Seweryniak, I. Wiedenhöver, M. P. Carpenter, R. V. F. Janssens, T. L. Khoo, T. Lauritsen, C. J. Lister, and P. Reiter, *Phys. Rev. C* **65**, 017302 (2001).
- [91] A. Gargano, *Eur. Phys. J. A* **20**, 103 (2004).
- [92] L. Coraggio, A. Covello, A. Gargano, N. Itaco, and T. T. S. Kuo, *Phys. Rev. C* **66**, 064311 (2002).
- [93] I. Talmi, *Simple Models of Complex Nuclei* (Harwood, Chur, 1993).
- [94] T. Otsuka, T. Suzuki, R. Fujimoto, H. Grawe, and Y. Akaishi, *Phys. Rev. Lett.* **95**, 232502 (2005).
- [95] Y. Utsuno, T. Otsuka, B. A. Brown, M. Honma, T. Mizusaki, and N. Shimizu, *Phys. Rev. C* **86**, 051301(R) (2012).